Two-Dimensional Simulation of Frost Formation on the NACA0012 Airfoil under Strong Convection by Using the P-VOF Method

Bin Xia
Tsinghua University https://orcid.org/0000-0003-2511-8809
Xianghua Xu (xxh@tsinghua.edu.cn)
Tsinghua University
Xingang Liang
Tsinghua University

Research Article

Keywords: frosting, simulation, airfoil, VOF, strong convection

Posted Date: June 2nd, 2021

DOI: https://doi.org/10.21203/rs.3.rs-557402/v1

Version of Record: A version of this preprint was published at Advances in Aerodynamics on July 15th, 2021. See the published version at https://doi.org/10.1186/s42774-021-00075-w.

Two-Dimensional Simulation of Frost Formation on the NACA0012 Airfoil under Strong Convection by Using the P-VOF Method

Bin Xia[1,2] , Xianghua Xu [1*], Xingang Liang[1]
(1: Key Laboratory for Thermal Science and Power Engineering of Ministry of Education, School of Aerospace Engineering, Tsinghua University, Beijing 100084, China;
2: State Key Laboratory of Aerodynamics, China Aerodynamics Research and Development Center, Mianyang, 621000, China)

*Correspondence: xxh@tsinghua.edu.cn

Abstract: A newly developed frosting simulation method, pseudo-VOF (p-VOF) method, has applied to simulate the dynamic frost formation on the NACA0012 airfoil under strong convection. The p-VOF method is a pseudo volume of fraction simulation method of the multiphase flow with phase change. By solving a simplified mass conservation equation explicitly instead of the original volume fraction equations in CFD software, the efficiency and robustness of calculation are greatly improved. This progress makes it possible to predict a long-time frost formation. The p-VOF method was successfully applied to the simulation of dynamic frosting on the two-dimensional NACA0012 airfoil under strong convection conditions with constant frost physical properties. The simulation result shows that the average thickness of the frost layer increases, and the frost bulges and flow separation appear earlier, when the airfoil surface temperature decreases or the air humidity increases. The frost bulges and flow separation appear earlier, when the air velocity is faster, the growth rate of the frost layer at the early stage is greater, but the final frost layer is thinner.
Keywords: frosting, simulation, airfoil, VOF, strong convection

1 Introduction

When The aircraft cruise at high altitude where the ambient temperature is well below freezing, the fuel in the wing tanks could be cooled to below freezing point [1]. If the aircraft flies into a warm, humid airspace immediately, the water vapor in the air may desublimate on the surface of the wing. This frost phenomenon usually occurs when the aircraft descends from the cruise altitude to land. The frosting on the wing is different from the icing on the wing. The icing on the wing is the process of liquid water turning into solid ice when the supercooled water drops hit the wing[2-4], while the frosting on the wing is the process of water vapor desublimate into solid frost on the

cold wing. The wing frosting has not received enough attention and there is a few public researches of the desublimation frosting on the wing [1, 5], although there have been many studies on aircraft icing.

The frost on the wing surface will change the roughness of the skin and the shape of the wing, resulting in change of the lift-drag ratio even the airflow separation behavior [6], thereby affecting the aerodynamic performance of the aircraft. For energy saving and flight safety requirements, the importance of wing frosting studies has become increasingly prominent. It is necessary to predict the frost formation on the wing in different flight environments and evaluate its possible adverse effects firstly. The wing frosting is the problem of the desublimation frost on the cold surface under strong convection conditions.

In order to predict the frosting behavior on cold surface, several numerical models have been developed, which can be divided into three categories. The first type is one-dimensional model, which uses empirical correlations obtained from experiments to calculate the heat transfer coefficient and mass transfer coefficient on the frost surface[7-9]. Nevertheless, the one-dimensional models cannot reflect the characteristics of complex surface shape, and are usually applied to the researches of frosting on cold plate [10]. Moreover, this type models do not solve the coupled flow and heat transfer problems in air and frost, so it cannot be used to predict the frost formation under changing flows with frosting. The second type of models solves the flow, heat and mass transfer within the air, the heat and mass transfer within the frost layer, which is regarded as a solid region [11-13]. This type models solves the governing equations in air domain and frost domain respectively. The third type of models uses the multi-phase flow method to solve the flow, heat and mass transfer simultaneously in humid air and frost layer with the same set of governing equations. Current researches often adopt the VOF model [14, 15] and the Eulerian model [16, 17]. The multiphase flow model requires the least empirical correlations and assumptions, so it is more suitable for the simulation of frosting in actual working conditions. However, those researches only studied the simulation of frosting under natural convection or low velocity flow conditions.

According to the frosting experiment on the cold plate under strong convection[18], it was found that when the flow velocity is faster than 10m/s that was much faster than the flow velocity in the refrigeration systems, the frost layer is compact. Under strong convection, the new desublimated water vapor mainly contributes to the increase of the frost thickness, rather than increases the density of frost layer. However, the desublimated water vapor increases both the thickness and the density of the frost layer under low airflow velocity [10]. As the frosting progresses, the frost surface temperature gradually increases, and when the water vapor content in the humid air is equal to the saturated water vapor content at the frost surface temperature, the water vapor in the humid air will stop to change into frost. If the water vapor content in the humid air is lower than the saturated water vapor content at 273.15K, the frost surface temperature cannot reaches to 273.15K, and no liquid water will appear on the frost surface. This kind of desublimation frosting processes under these humidity conditions was called as dry mode frosting [18].

This paper developed a new multi-phases flow method, p-VOF method, to simulate the dry mode frosting on the NACA0012 airfoil under strong convection conditions.

2 P-VOF method for frosting simulation

The p-VOF method is a pseudo volume of fraction method of multiphase flow simulation, which solves a simplified mass conservation equation to obtain the volume fraction change of frost phase explicitly instead of the original volume of fraction (VOF) equations in CFD software to improve the calculation efficiency and robustness. This progress makes it possible to predict a long-time frost formation. This method does not solve the volume fraction equation in original VOF method, so it is called pseudo-VOF (p-VOF) method.

According to the observation of experiments [18], the assumptions for simulation are as follows:

- The humid air is an incompressible Newtonian fluid with constant properties.
- The phase change between water vapor and frost occurs only on the frost surface (or the airfoil surface at the initial moment).
- When the frost surface temperature is lower than the freezing point, if the water vapor content is greater than the saturated water vapor content on the frost surface, water vapor desublimates into frost, and vice versa.
- The mass transfer inside the frost is neglected because the frost layer formed under strong convection is dense.

Humid air is set to be the primary phase and frost is the secondary phase. Humid air is multi-component which composes of dry air and water vapor. The VOF model calculate the mass, momentum, energy transport and water vapor diffusion by equations as shown in Eqs. (1), (2), (3) and (4) respectively,

$$\frac{\partial}{\partial t}\left(\alpha_i \rho_i\right)+\nabla\cdot\left(\alpha_i \rho_i \vec{u}\right)=S_{mi}, \tag{1}$$

$$\frac{\partial}{\partial t}\left(\rho \vec{u}\right)+\nabla\cdot\left(\rho \vec{u}\vec{u}\right)=-\nabla p+\nabla\cdot\left[\mu\left(\nabla \vec{u}+\nabla \vec{u}^{T}\right)\right]+\vec{F} \tag{2}$$

$$\frac{\partial}{\partial t}\left(\rho E\right)+\nabla\cdot\left(\vec{u}\left(\rho E+p\right)\right)=\nabla\cdot\left(k_{eff}\nabla T\right)+S_h \tag{3}$$

$$\frac{\partial}{\partial t}\left(\alpha_a \rho_a w\right)+\nabla\cdot\left(\alpha_a \rho_a w\vec{u}\right)=\nabla\cdot\left(\rho_a D_{H_2O}\nabla w\right)+S_{mf} \tag{4}$$

where ρ is the density, p is the pressure, $\vec{u}$ is the velocity vector, t is the frosting time, α is the volume fraction, S_m is the mass source/sink term due to phase change. subscript i is a or f, representing the humid air phase or the frost phase. The sum of volume

fractions of two phases is 1, as shown in Eq. (5),

$$\alpha_a + \alpha_f = 1, \tag{5}$$

and $\vec{F}$ is the body force or momentum source, μ is the viscosity and k_{eff} is the effective thermal conductivity of the mixture, ρ, μ and k_{eff} can be calculated by sum of each phase weighted by volume fraction. T is the temperature and S_h is the heat released or absorbed during phase change. E is the internal energy of the two-phase mixture, which is mass–averaged by phase fraction. w is the mass fraction of the water vapor in humid air, D_{H_2O} is the diffusion coefficient of water vapor in humid air.

Because the frost phase does not move after it generated and the frost surface changes only when desublimation or sublimation occurs, the convective term (the second term on the left) of volume fraction in Eq. (1) can be ignored. Eq. (1) can be simplified to

$$\frac{\partial}{\partial t}\left(\alpha_f \rho_f\right) = S_{mf}. \tag{6}$$

At the phase interface, the source term can be calculated by the mass transfer rate from water vapor in humid air to frost, which is determined by the kinetic theory [19],

$$S_{mf} = -\frac{2\sigma}{2-\sigma}\frac{1}{\sqrt{v}}\sqrt{\frac{R_w T}{2\pi}}\left(\rho_v - \rho_s(T)\right), \tag{7}$$

where σ is the coefficient of correction and 0.03 is suggested for water [19]; v is the volume of the mesh cell. R_w is the water vapor gas constant, which equals to 461.5 J/(Kg·K); ρ_v is the density of water vapor, ρ_s is the saturated density of water vapor at the phase interface corresponding to T at the phase interface.

Source term S_h in energy Eq. (3) is the latent heat released or absorbed due to phase change, which is not zero only at the phase interface

$$S_h = S_{mf}\gamma, \tag{8}$$

where γ is the latent heat of phase change.

The transient two-dimensional frosting process is simulated by using ANSYS FLUENT with VOF multiphase flow model. The flow chart of simulation is shown in Fig. 1.

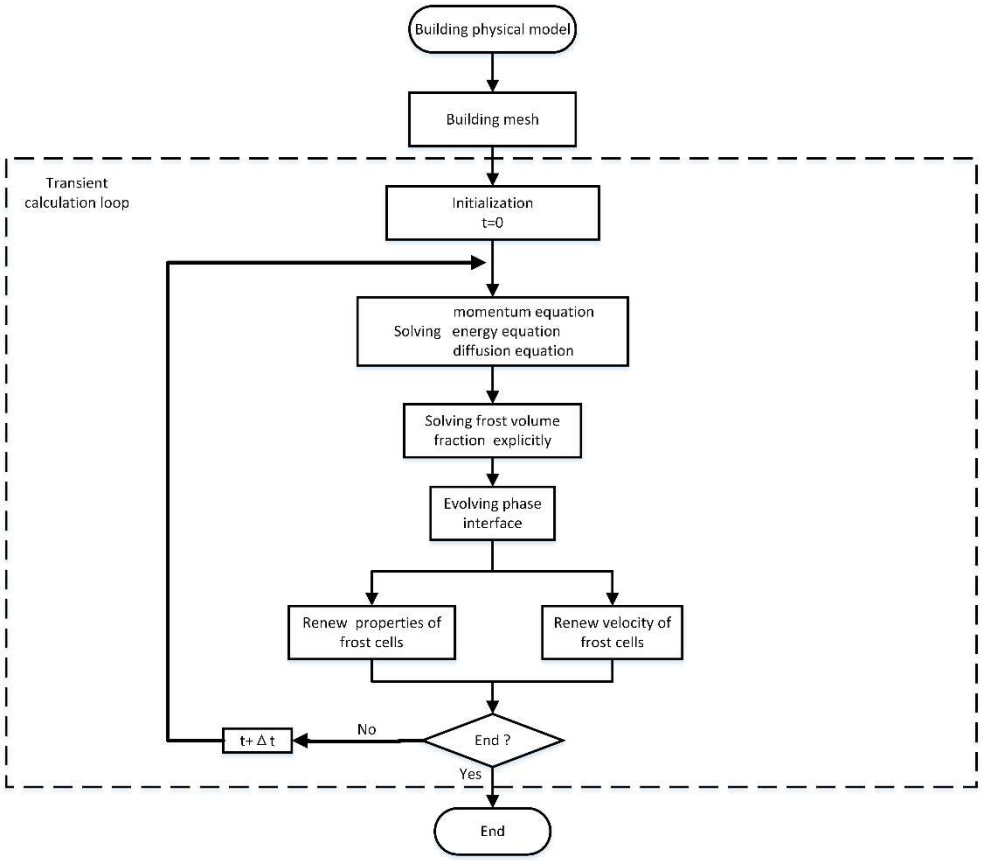

Fig. 1 Flow chart of simulation

The PISO algorithm is chosen to couple the pressure and velocity. The pressure is discretized by the PRESTO! method. At each time step, the change of frost volume fraction at the phase interface is determined only by explicitly solving

$$\Delta\alpha_f = \frac{\Delta t}{\rho_f} S_{mf}, \tag{9}$$

which is transformed from Eq.(6), where Δt is the time step, $\Delta\alpha_f$ is the variation of the frost volume fraction during Δt. By explicitly solving Eq. (9) instead of the original VOF equations of FLUENT (Eq. (1)), the efficiency and robustness of calculation can greatly improve. If the phase interface temperature $T > 273.15$ K, there is no growth of frost, and $\Delta\alpha_f$ is set to 0.

The calculation of source terms, searching for phase interface cells, and the evolution of volume fraction are implemented by employing UDFs (user-defined functions), which are hooked to ANSYS FLUENT. It should be noted that since the original VOF equation of FLUENT is not solved, the software has data transmission problems in the assignment of the thermal conductivity and viscosity of the mixture. Therefore, it is necessary to use UDFs to assign the thermal conductivity and viscosity of the mixture to the humid air phase in order to simulate frosting correctly.

3 Frosting simulation on the two-dimensional airfoil

In order to verify the applicability of the p-VOF method for dynamic desublimation frosting on airfoil under strong convection conditions, simulations on NACA0012 are carried out under different air velocity, air humidity and airfoil surface temperature conditions with constant frost physical properties. The frost density uses 560 kg/m^3 and frost thermal conductivity uses 0.2 W/m·K. The chord length of airfoil is 10mm. The simulation conditions are in Table 1. The maximum Reynolds number of these conditions is 4×10^4 , so the laminar model is used.

Table 1 Conditions of frosting simulations

Parameters	Value
Air temperature / K	310
Air velocity / (m/s)	10, 50
Relative humidity / %	7, 9
airfoil surface temperature / K	230, 250

The mesh of the computation region is shown in Fig. 2. The half model is used to reduce the burden of computation. The grids is refined near the airfoil surface. The length (X direction) of the mesh cell on the surface of airfoil is 1 mm. A boundary layer is attached to the airfoil surface with first layer of 0.01 mm and increasing ratio of 1.007 (Y direction). The airfoil surface is set to isothermal wall condition.

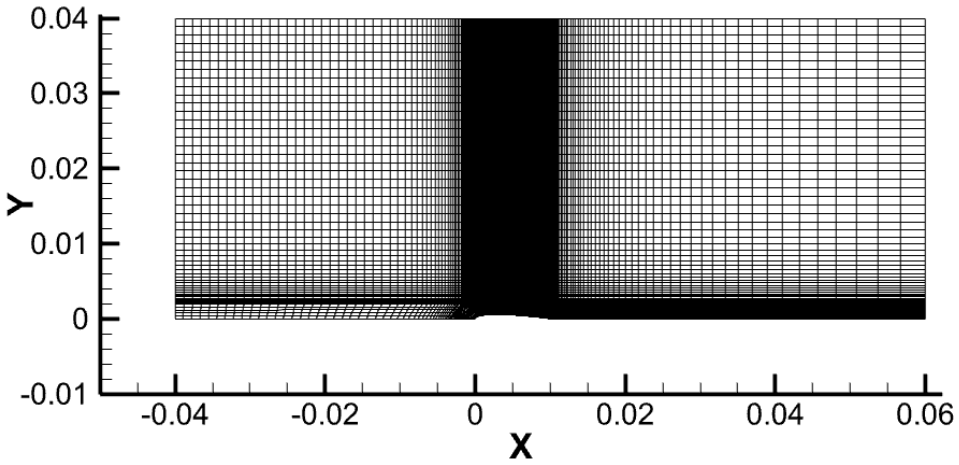

Fig. 2 Mesh for frosting simulation on airfoil

3.1 Dynamic desublimation frosting on airfoil

The baseline condition is set for the simulation: the airfoil surface temperature 250 K; the air velocity 10 m/s; the air temperature 310K and the relative humidity 7%. The frosting duration is 30 minutes. The average thickness curve of the frost layer is shown in Fig. 3, and the average thickness of the frost layer at the end of 30 minutes is 0.43mm.

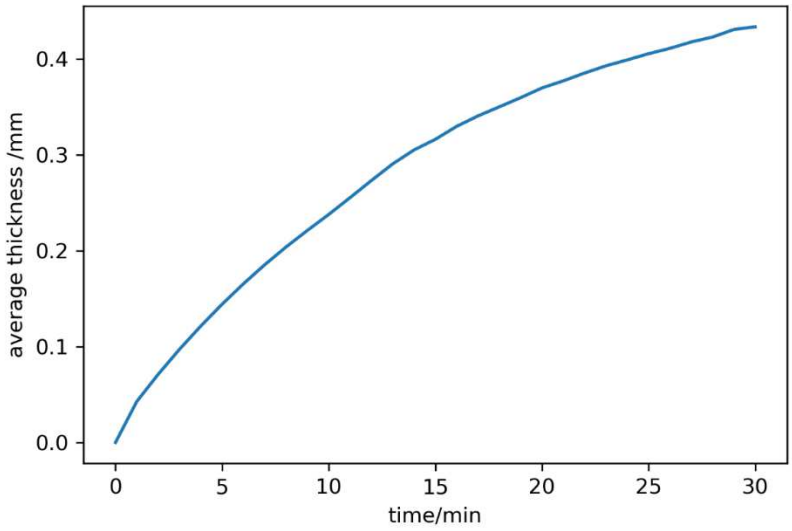

Fig. 3 Average frost layer thickness varying with time under baseline state condition

Under the baseline condition, the frost morphology at different instant is shown in Fig. 4. The flow direction is from left to right. The frost layer thickness is relatively uniform on the airfoil in the early stage of frosting. Only the frost layer close to the leading edge of the wing is slightly thicker than the frost on the other parts of the airfoil. As the frosting progresses, the frost layer gradually thickens. At the 15th minute, a slight bulge appears in the front of the frost layer. Then the bulge becomes more and more obvious, and some new smaller bulges continue to form on the frost surface afterwards.

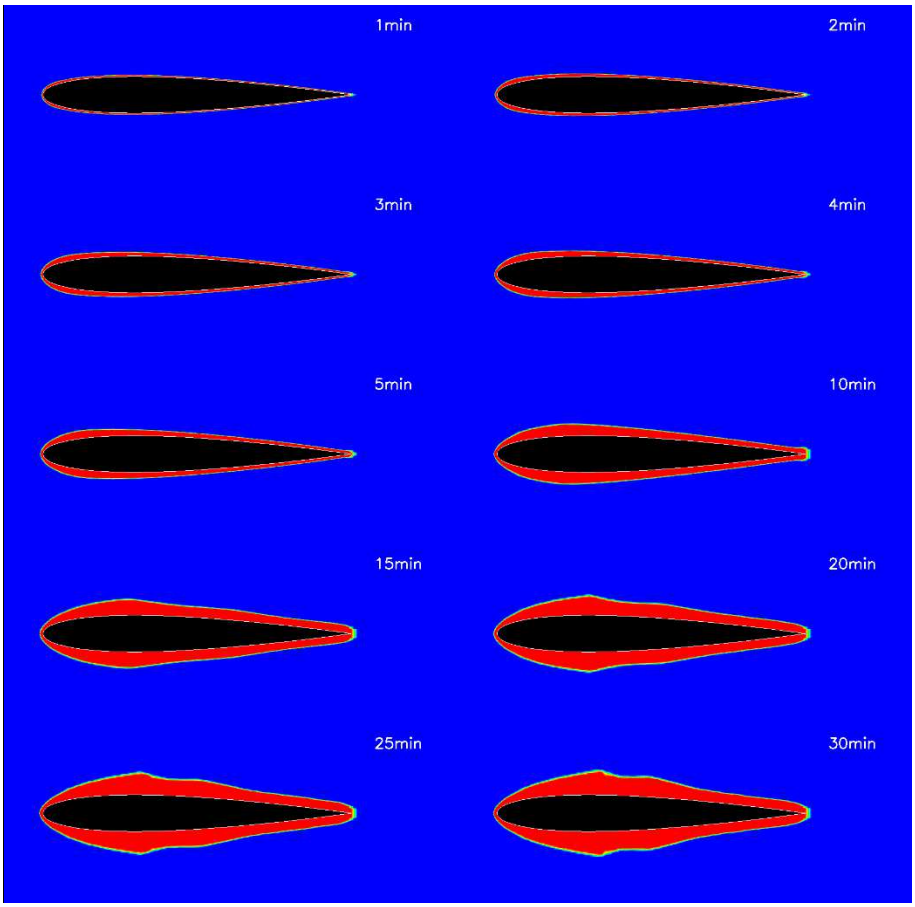

Fig. 4 The morphology of the frost layer on the airfoil varying with time

The velocity field and velocity vector field varying with time are shown in Figs. Fig. 5 andFig. 6, respectively. At the 5th minute, the flow on the airfoil surface still attaches to the surface. At the 10th minute, flow separation has occurred near the rear of the airfoil, and vortices appear. At the 20th and 30th minute, the flow separation and vortices on the airfoil surface are more obvious and regular. A series of small to large vortices can be clearly distinguished from the velocity vector figure.

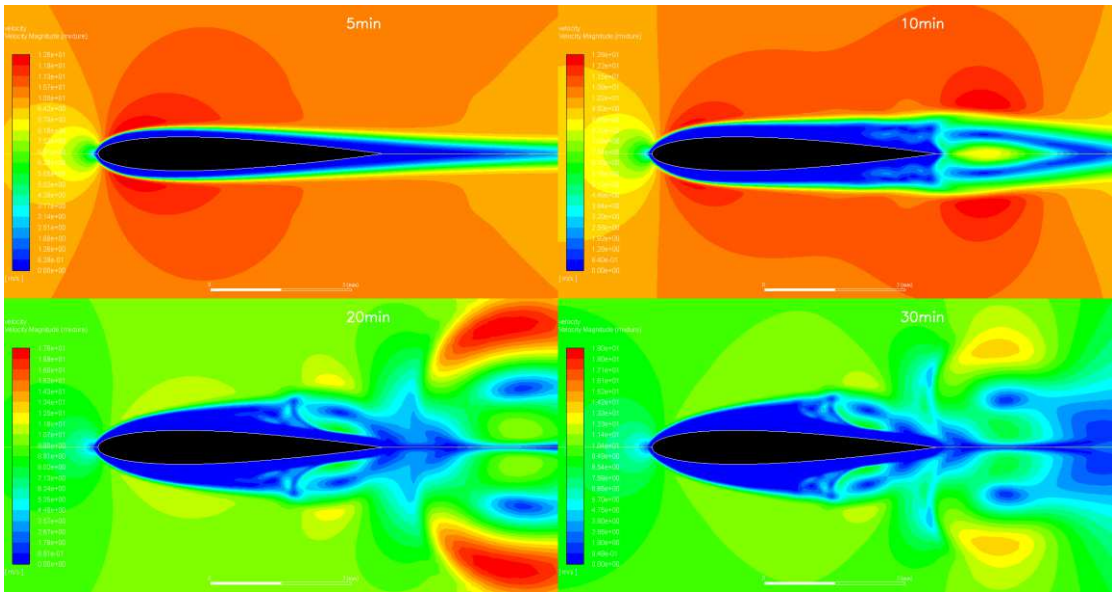

Fig. 5 Velocity field changes with the frosting on airfoil

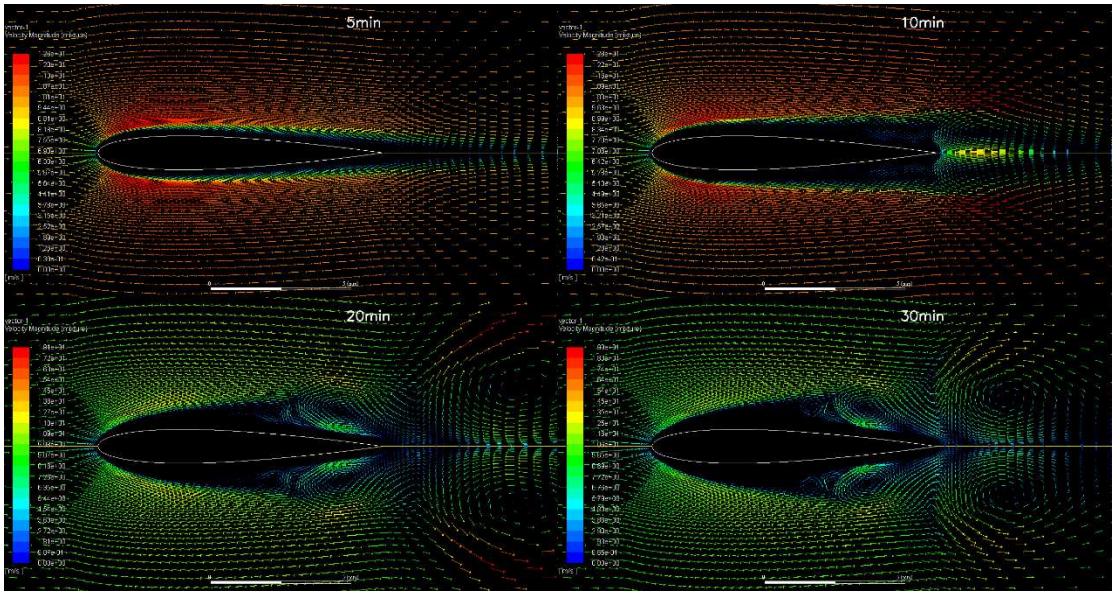

Fig. 6 Velocity vector field changes with the frosting on airfoil

Fig. 7 shows the temperature field at different time. At the 5th minute, the temperature boundary layer on the airfoil still maintains an attached flow. At the 10th

minute, the temperature boundary layer at the rear of the airfoil thickens and develops some low-temperature air zones in the shape of eddy current at the tail of the airfoil. At the 20th and 30th minutes, from the position of the frost bulge, some clear vortices of low-temperature air appear.

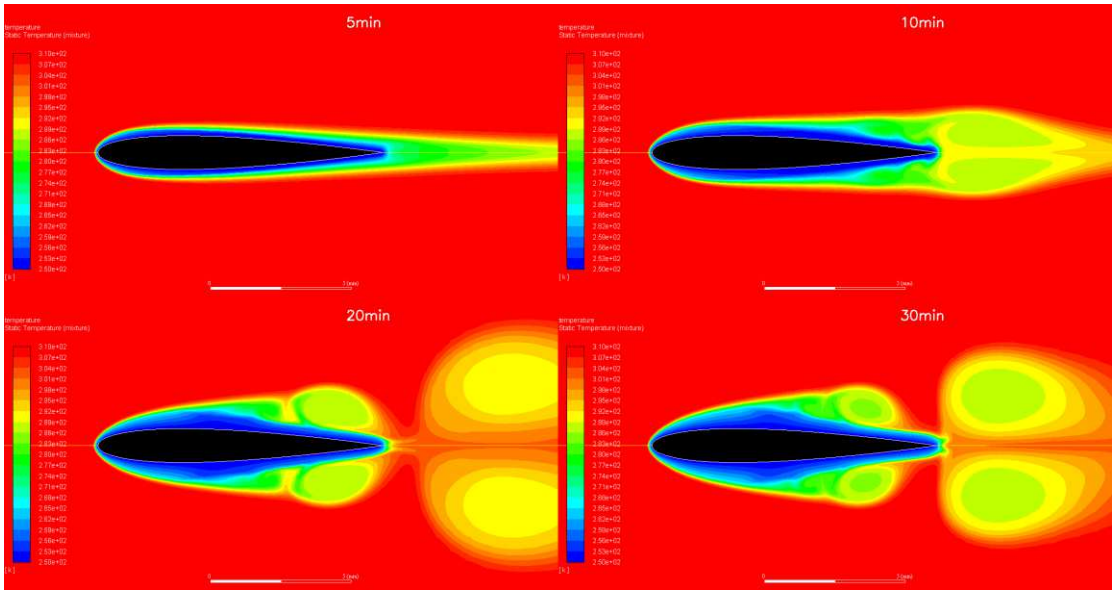

Fig. 7 Temperature field of two-dimensional airfoil surface varying with time

The moisture content of the air near the frost layer changes is shown in Fig. 8. Before 10 minutes, there are obvious areas with low water vapor content near the frost layer, especially near the rear of the airfoil. After 20 minutes, there are only some low humidity areas on the leeward side of the frost layer bulges, indicating that the frost layer areas in other locations have almost reached the mass transfer balance.

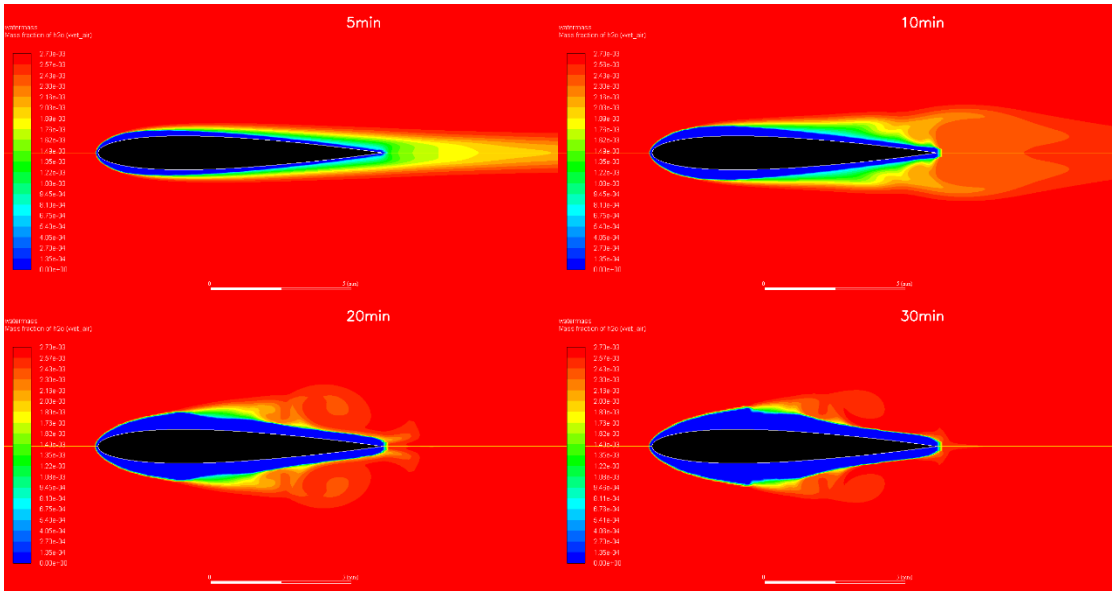

Fig. 8 Water vapor content change in the air with the frosting on airfoil

3.2 The influence of air velocity on frosting

The dynamic frosting behaviors on the two-dimensional airfoil under different air velocities are simulated and compared. The variation of the average thickness of the frost layer under different air velocities is shown in Fig. 9. The higher the air velocity, the faster the growth rate of the frost layer at early stage, but the earlier the frosting rate begins to decrease significantly, and the thinner the final average thickness of the frost layer will be.

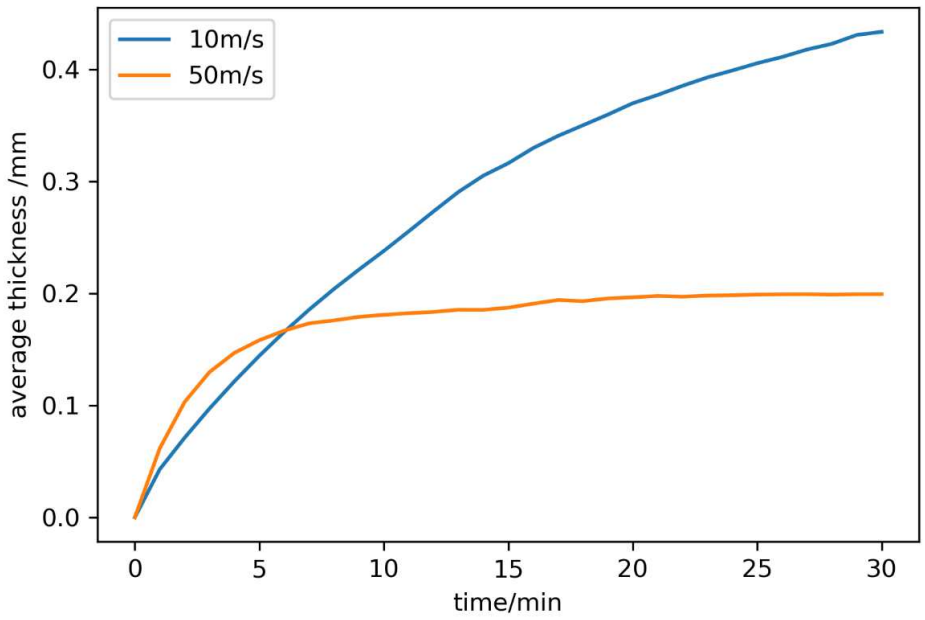

Fig. 9 Variation of the average thickness of the frost layer under different air velocities

The change of the frost layer morphology on the airfoil surface under different flow velocity conditions are shown in Fig. 10. The frost layer morphology difference under different air velocities are quite obvious. The first bulge position of the frost layer under 50m/s is more rearward than that under 10m/s, as can be seen from the comparison of the frost layer morphology at the 5th minute in the figure. The morphology of the frost layer at 50 m/s did not change significantly after 10 minutes, while the morphology of the frost layer kept changing at a lower speed of 10 m/s.

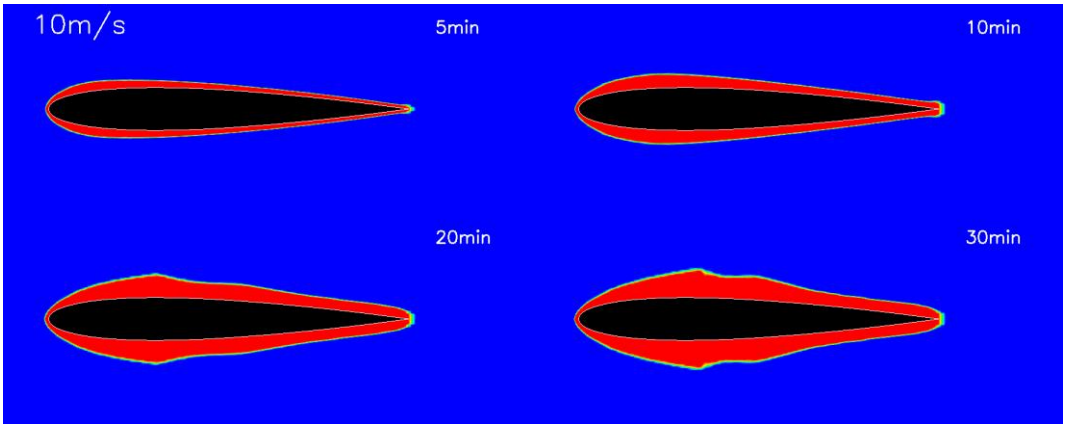

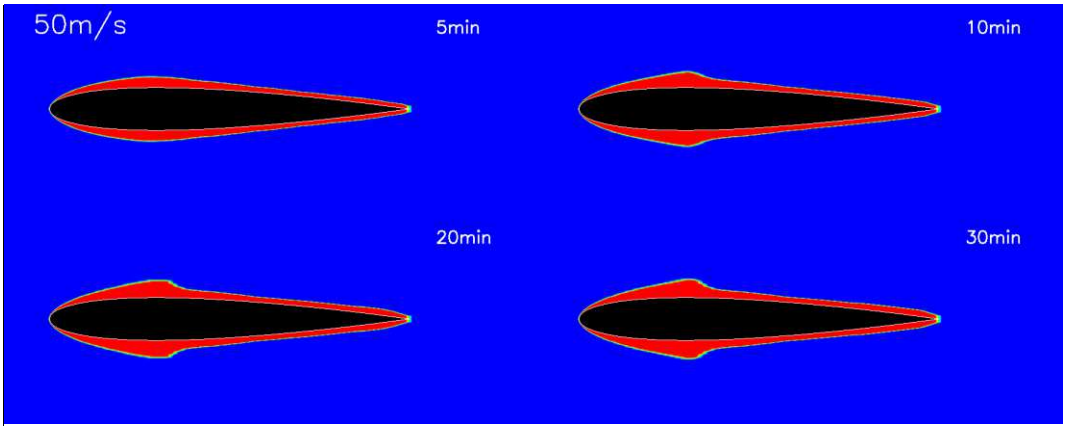

Fig. 10 Frost layer morphology varying with time under different air velocities

The velocity vector field varying with time under different air velocities are shown in Fig. 11. It can be clearly seen from the figure that the flow on the frost surface has appeared obvious vortex sequence at the 5th minute under the incoming airflow velocity of 50 m/s.

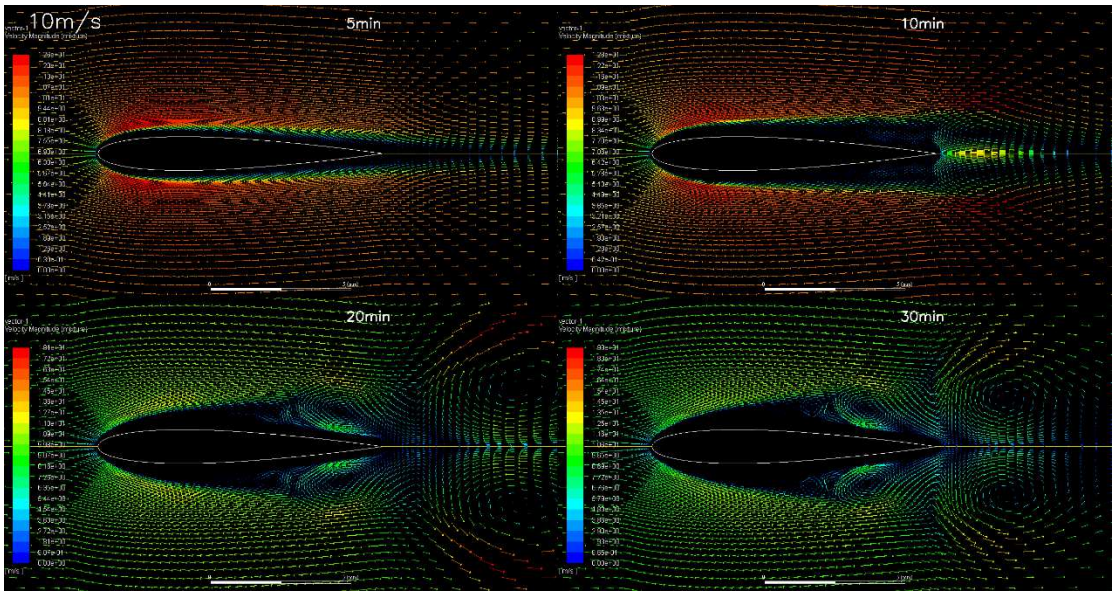

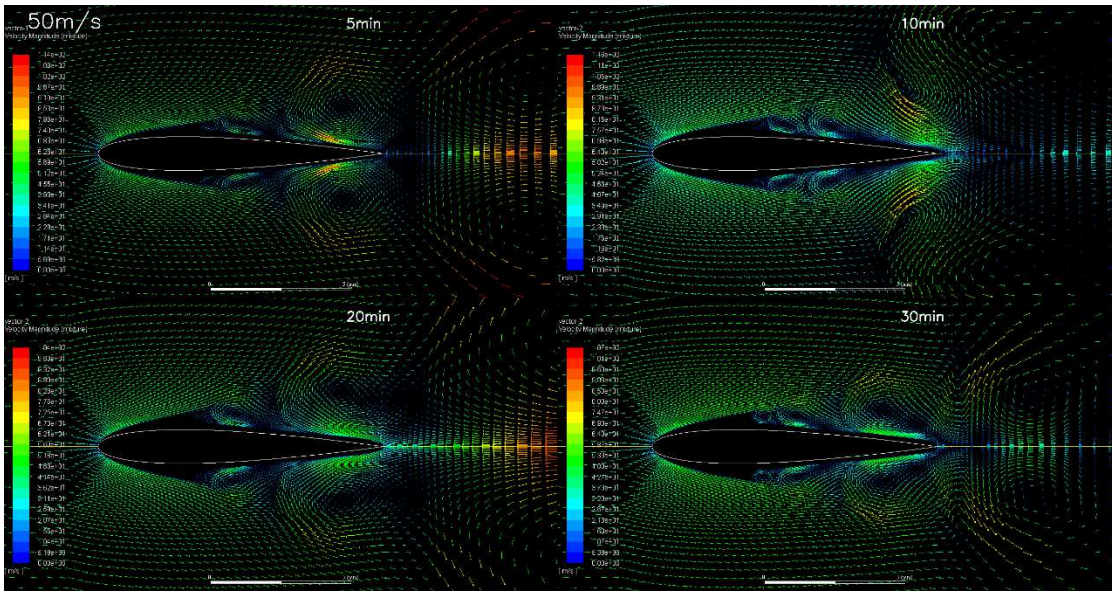

Fig. 11 Velocity vector field varying with time under different air velocities

The change in temperature field under different air velocities are shown in Fig. 12. Compared with the case of 10 m/s that maintain the attached temperature boundary layer at the initial stage of frosting, the flow on the surface of the frost layer has shown obvious low-temperature vortices sequence at the 5th minute under 50 m/s condition, which indicates the separation of flow.

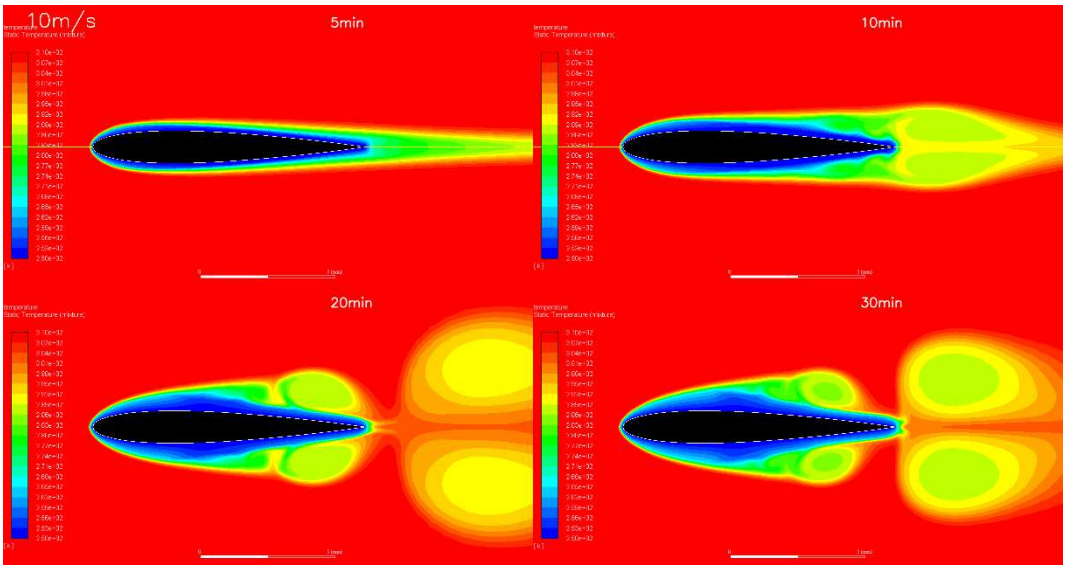

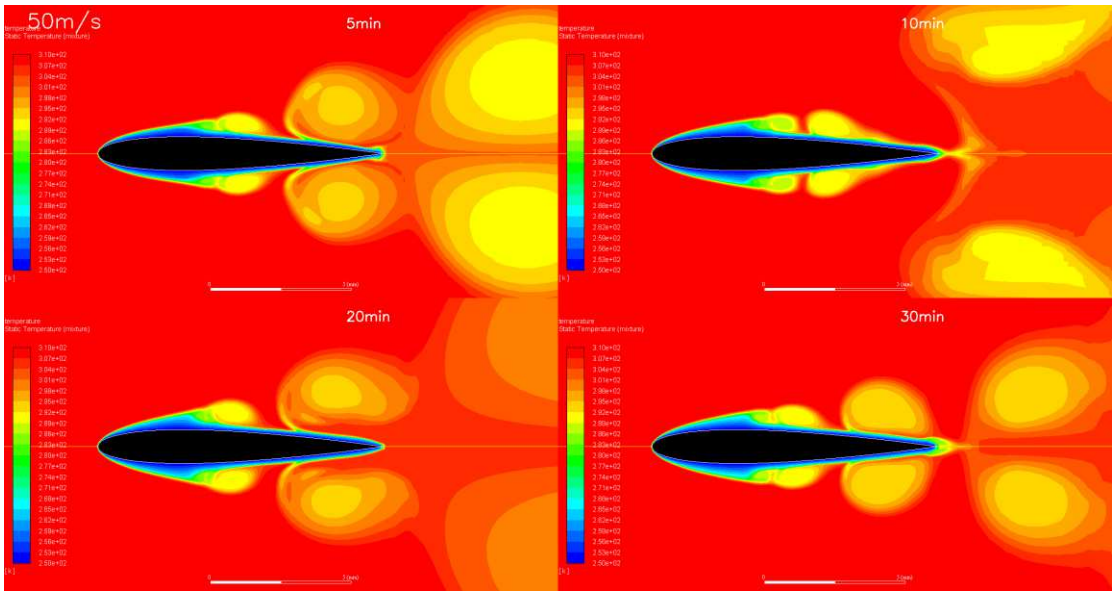

Fig. 12 Temperature field varying with time under different air velocities

3.3 The influence of air humidity on frosting

The frosting behaviors on the airfoil under different air humidity were simulated successfully. The change in average frost thickness with time under different humidity conditions is shown in Fig. 13. It can be seen from the curves that as the air humidity increases, the growth rate of the frost layer increases, and the average thickness of the frost layer increases in the same moment.

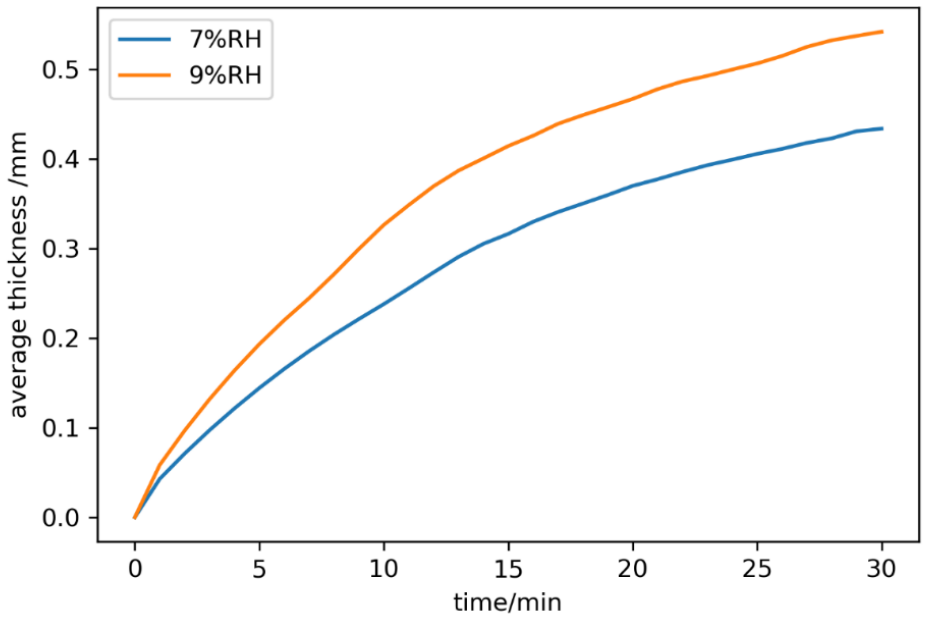

Fig. 13 Change in average frost thickness with time under different air humidity

The morphology change of frost layer with time under different air humidity conditions is shown in Fig. 14. Higher air humidity leads to greater frosting rate, and the thicker frost layer, which is consistent with the change of the average frost thickness

in Fig. 13 . Moreover, the higher the huimidity is, the earlier the obvious frost bulges appears, and the frost morphology change is more complicated.

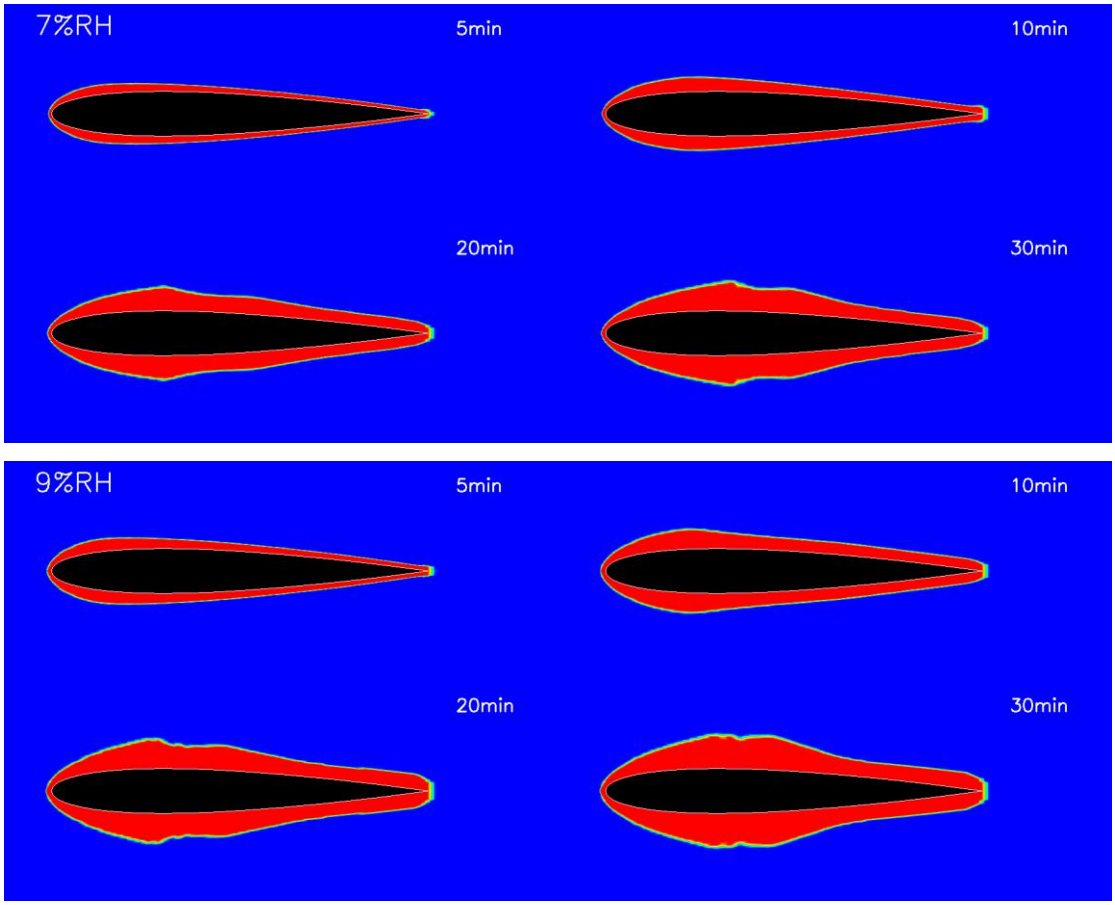

Fig. 14 The morphology change of the frost layer with time under different humidity

The velocity vector field varying with time under different air humidity are shown in Fig. 15. From the vortex sequence in the velocity vector field figure, it can be seen more clearly that the higher the incoming flow humidity, the earlier the flow separation occurs, which caused by the faster frost formation rate on the airfoil surface.

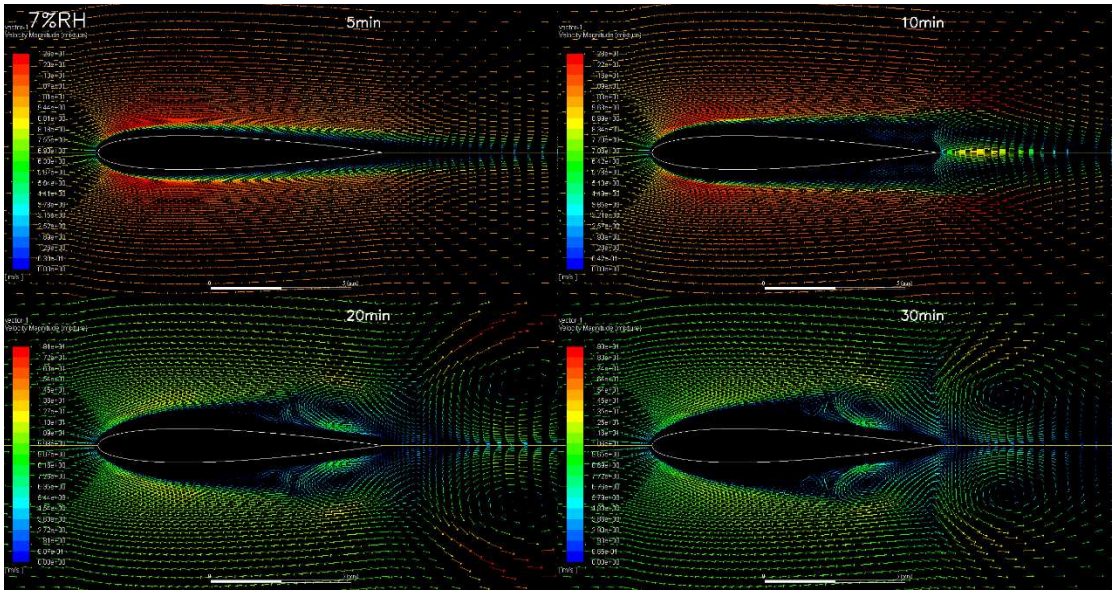

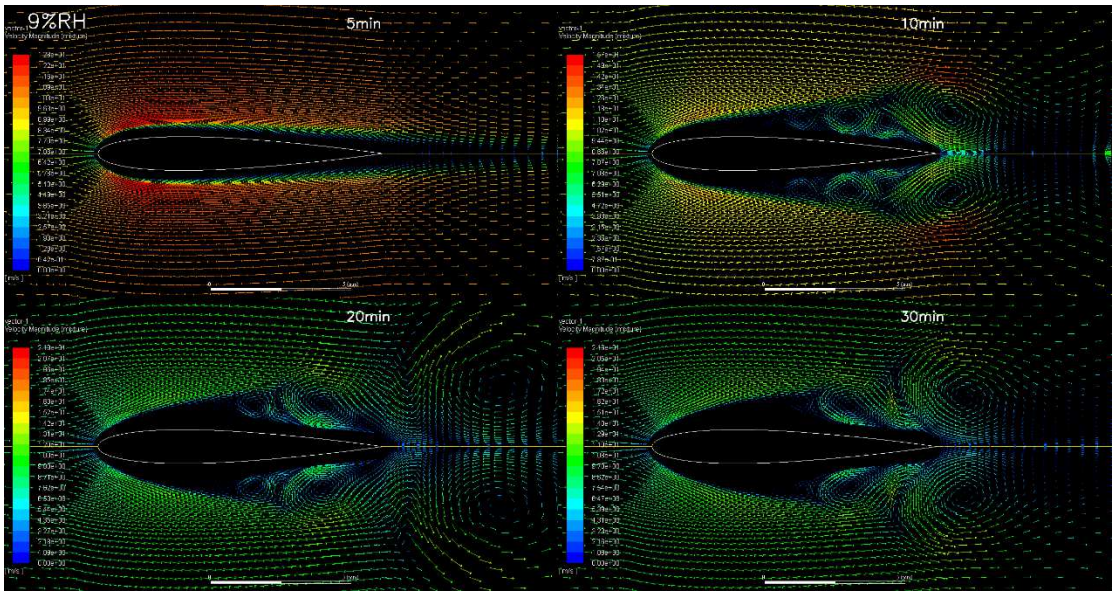

Fig. 15 Velocity vector field varying with time under different air humidity

The change of temperature field with time under different humidity conditions are shown in Fig. 16. The higher the air humidity, the earlier the occurrence of the low-temperature air masses caused by the vortex, which is a result of the morphology change of the frost layer.

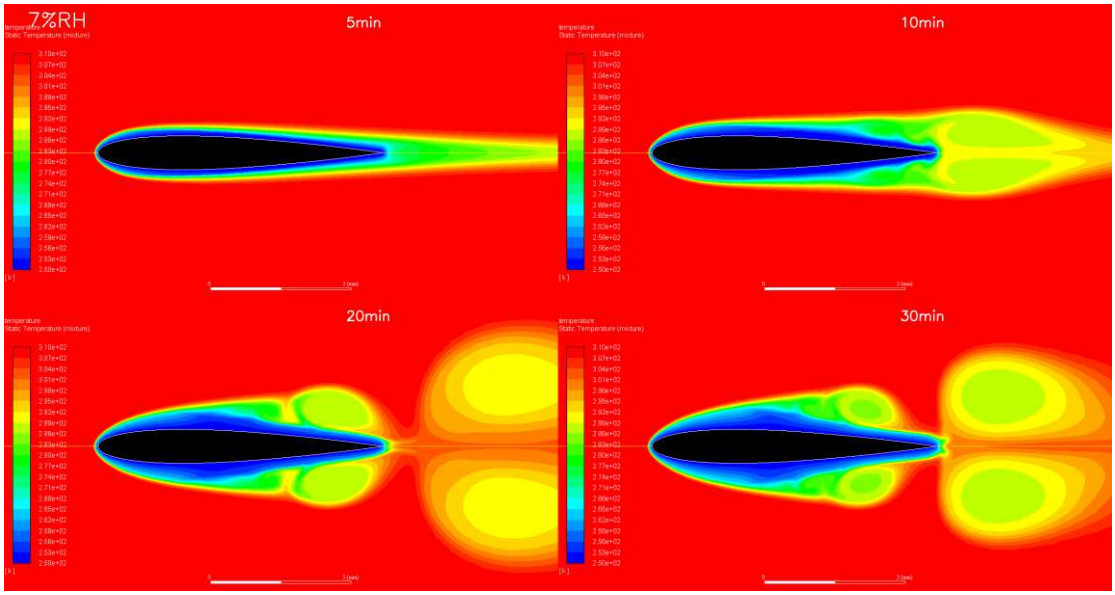

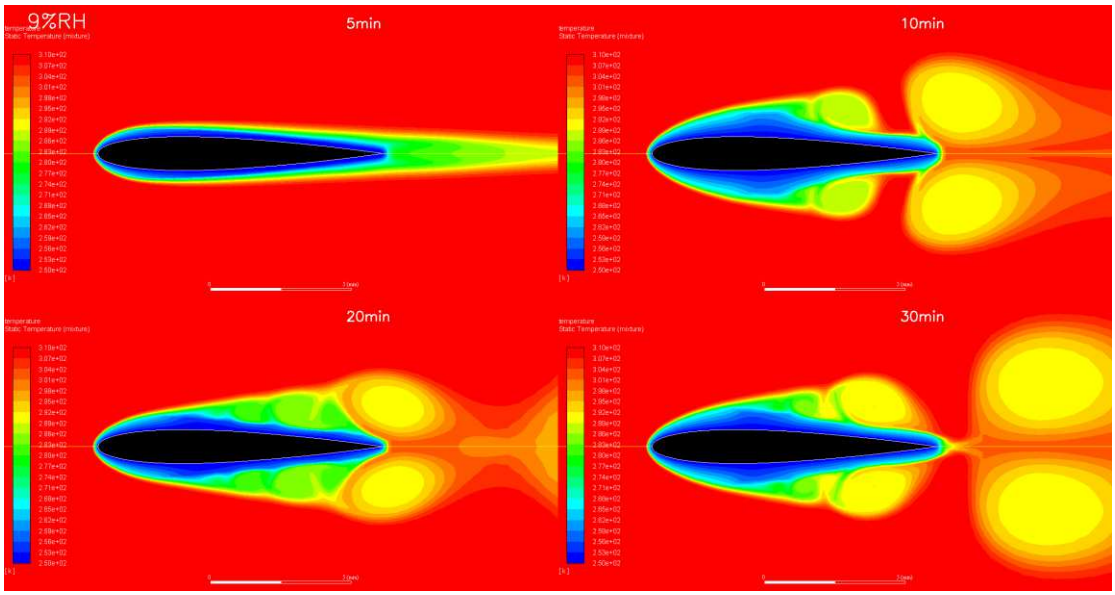

Fig. 16 Change of temperature field with time under different humidity conditions

3.4 The influence of airfoil surface temperature on frosting

The frosting simulations using the p-VOF method were carried out successfully under different airfoil temperatures. Fig. 17 shows the average thickness curves of the frost layer under different airfoil surface temperatures. The lower the airfoil surface temperature, the faster the frost layer grows, and the thicker the frost layer is in the same moment.

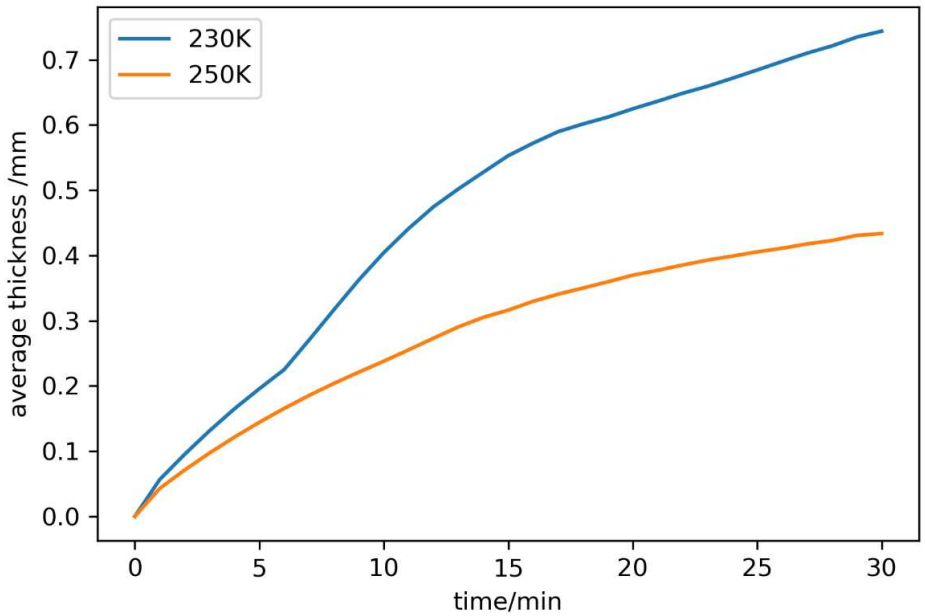

Fig. 17 The change of average frost thickness time under different airfoil surface temperatures

The development of the frost layer morphology under different airfoil surface temperatures is shown in Fig. 18. When the airfoil surface temperature is lower, the

frost formation rate is greater, and the frost layer is thicker on the airfoil. Moreover, when the temperature of the airfoil surface is lower, the frost bulges appears earlier and more obvious, and the bulges locate more close to the leading edge. After the bulges formed under the airfoil surface temperature of 230K, there are some holes wrapped in the frost layer at the position behind the first bulge location. This may be due to the greater frost formation rate and the relative lower water vapor replenishment by diffusion under such frosting condition, leading to the advantageous concentration effect of desublimation frost, which may be similar to porous structure of frost formed under natural convection and low speed flow conditions.

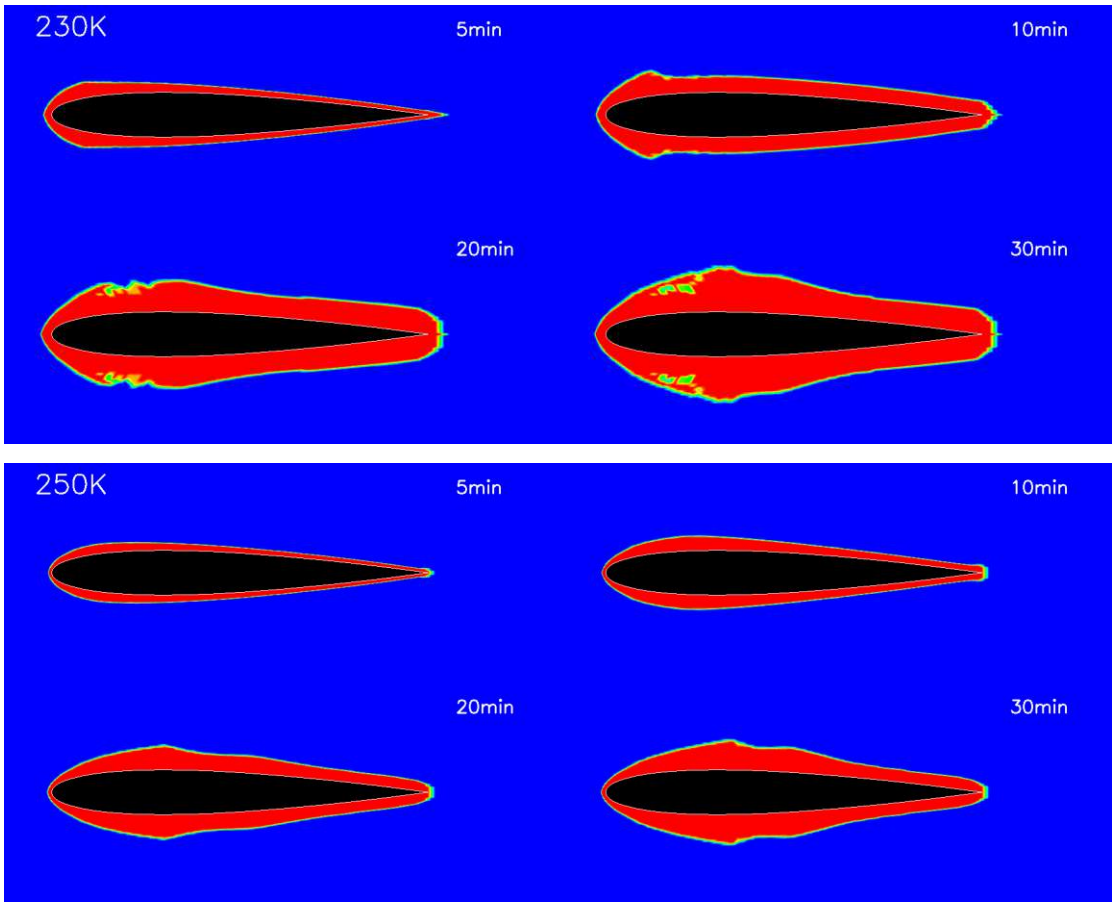

Fig. 18 The morphology of the frost layer varying with time under different airfoil surface temperatures

The influence of the frost layer morphology caused by different airfoil surface temperatures on flow separation can be seen clearly from the velocity vector field (shown in Fig. 19). It can be seen that the flow separation and the generation of vortices appear earlier due to the faster frost formation when the temperature of the airfoil surface is lower. Fig. 20 shows the temperature field under different airfoil surface temperatures. When the airfoil temperature is lower, the low temperature air zones caused by the airfoil flow vortex appears earlier. It can be found by comparing the temperature fields under different airfoil surface temperatures that the location of the frost layer bulges move forward, as well as the position where the vortices begin to separate when the surface is lower.

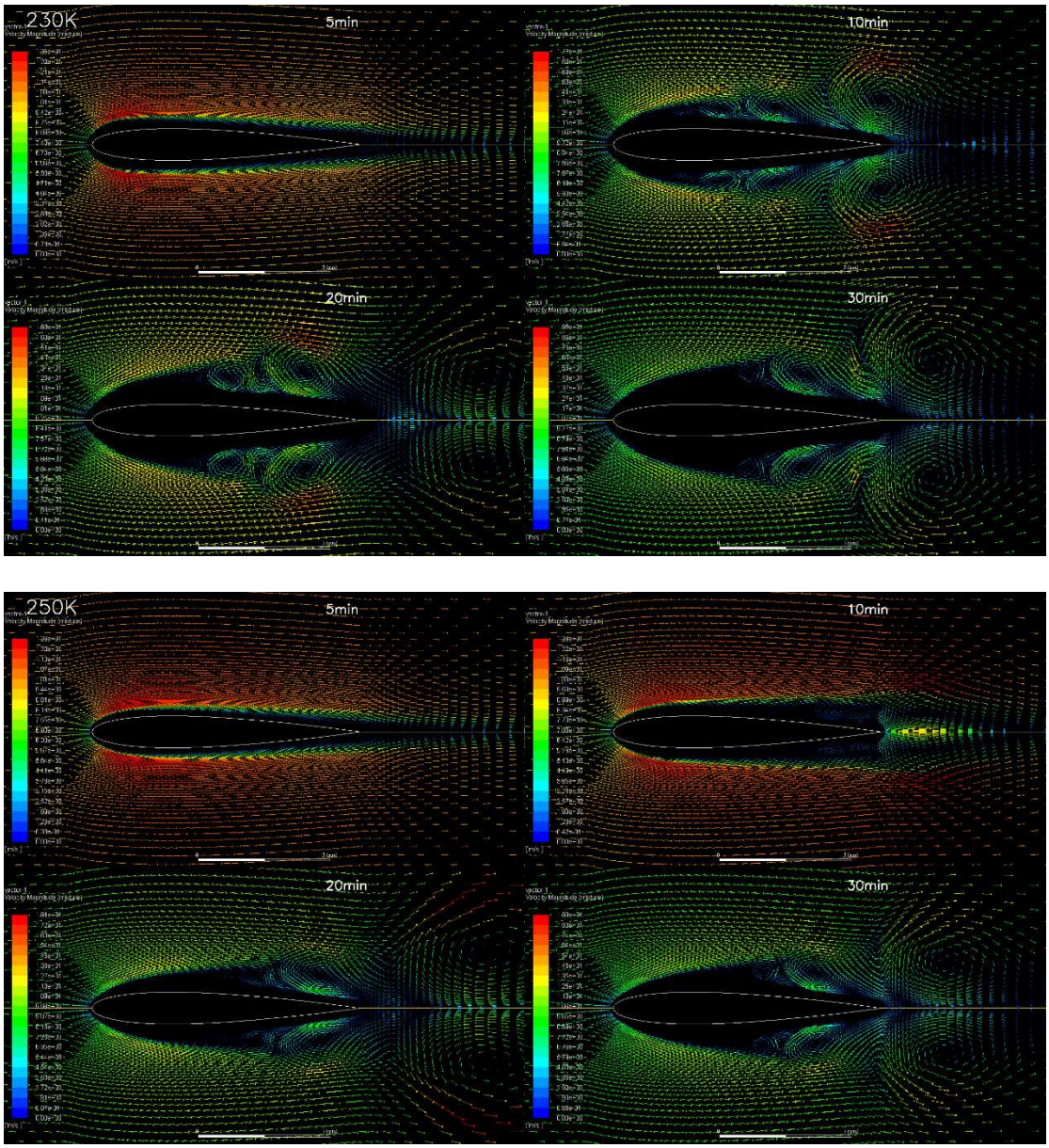

Fig. 19 Velocity vector field varying with time under different airfoil surface temperatures

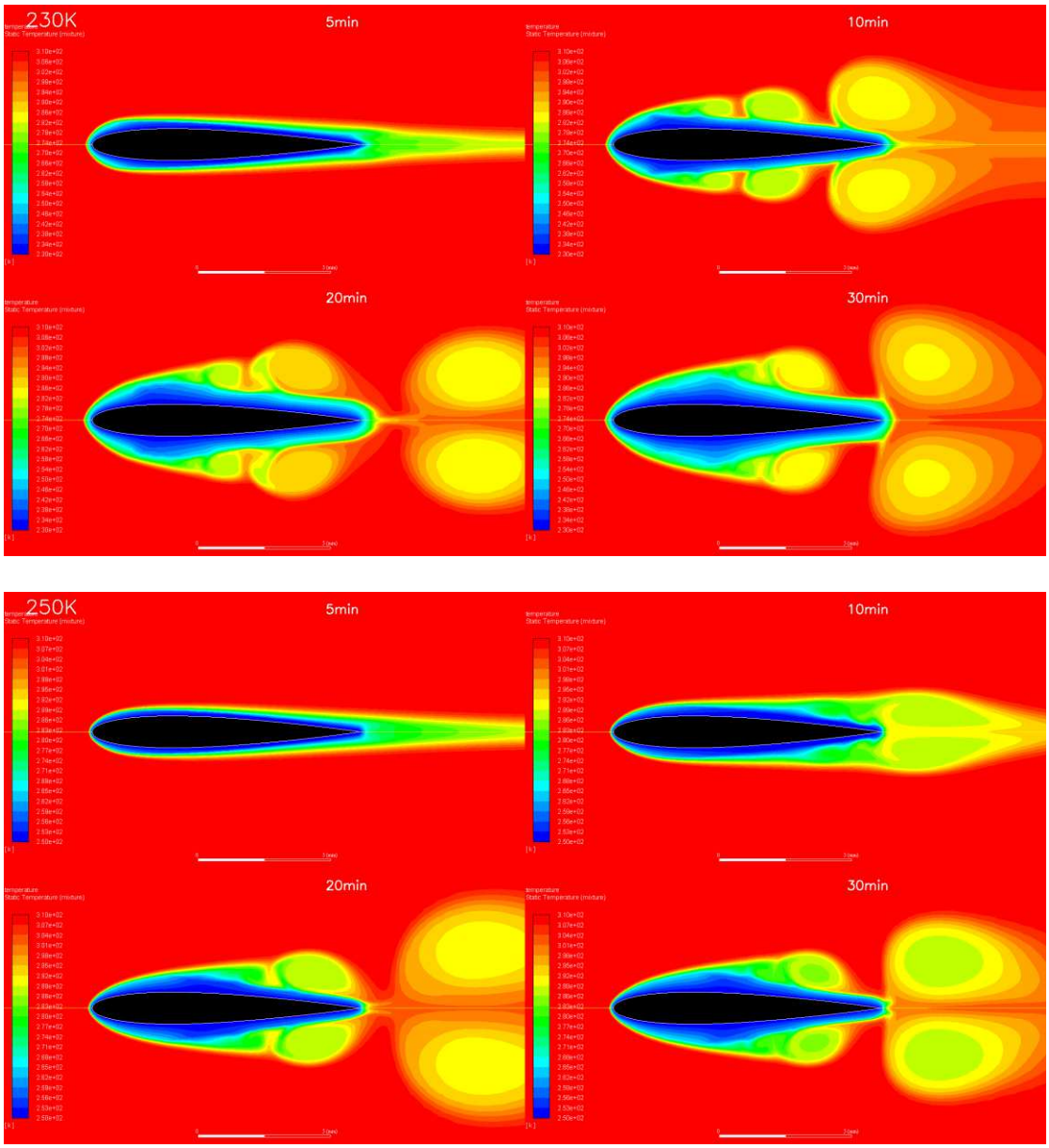

Fig. 20 Temperature field varying with time under different airfoil surface temperature

4 Conclusion

Through the above simulation, the following conclusions can be obtained:

1) The p-VOF method can be applied to conduct a stable and efficient numerical solution of dynamic desublimation frosting on the airfoil under different conditions.

2) The dynamic frosting process on the airfoil can be obtained clearly and vividly by using the p-VOF method. This method can be used to predict the frosting behavior on the airfoil.

3) The simulation result of frosting on the NACA0012 shows that the average thickness of the frost layer increases, and the frost bulges and flow separation appear earlier, with decrease of airfoil surface temperature or the increases of air humidity.

However, the frost bulges and flow separation appear earlier, when the air velocity is faster, the growth rate of the frost layer at the early stage is greater, but the final frost layer is thinner.

Acknowledgements

Not applicable

Authors' contributions

BX improved the p-VOF method, carried out the simulation, and was responsible for writing this manuscript. XX is the corresponding author of this paper who proposed the initial p-VOF method, and gave the instructions in keypoint of the research. XL guided the overall scheme of this research, and checked and modified the paper. The authors read and approved the final manuscript.

Author's information

BX is a Ph.D. student of the School of Aerospace Engineering (SAE) of THU and a senior engineer of CARDC. XX is a associate professor of the SAE of THU. XL is a distinguished professor of the SAE of THU and a senior expert in the field of heat and mass transfer.

Author details

[1] Key Laboratory for Thermal Science and Power Engineering of Ministry of Education, School of Aerospace Engineering, Tsinghua University, Beijing 100084, China.
[2] State Key Laboratory of Aerodynamics, China Aerodynamics Research and Development Center, Mianyang, 621000, China.

Funding

This research is financial supported by the National Numerical Wind-tunnel (NNW) Project

Availability of data and materials

The data and materials that support the findings of this study are available from the corresponding author upon reasonable request.

Competing interests

The authors declare that they have no competing interests.

References

1. Bragg MB, Heinrich DC, Valarezo WO, McGhee RJ (1994). Effect of underwing frost on a transport aircraft airfoil at flight Reynolds number. Journal of Aircraft, 31(6), 1372-9. doi:10.2514/3.46661.
2. Baumert A, Bansmer S, Trontin P, Villedieu P (2018). Experimental and numerical investigations on aircraft icing at mixed phase conditions. International Journal of Heat and Mass Transfer, 123, 957-78. doi:10.1016/j.ijheatmasstransfer.2018.02.008.
3. Zhou ZH, Yi X, Gui YW, Du YX (2015). Study on the Heat Transfer Characteristics in Aircraft Icing. Procedia Engineering, 99, 671-6. doi:10.1016/j.proeng.2014.12.588.
4. Du Y, Gui Y, Xiao C, Yi X (2010). Investigation on heat transfer characteristics of aircraft icing including runback water. International Journal of Heat and Mass Transfer, 53(19-20), 3702-7. doi:10.1016/j.ijheatmasstransfer.2010.04.021.
5. Dietenberger M (1981). Simulated aircraft takeoff performance with frosted wings. (Paper presented at the 19th Aerospace Sciences Meeting)
6. Bragg M, Gregorek G (1989). Environmentally induced surface roughness effects on laminar flow airfoils - Implications for flight safety. (Paper presented at the Aircraft Design and Operations Meeting)
7. Lee YB, Ro ST (2005). Analysis of the frost growth on a flat plate by simple models of saturation and supersaturation. Experimental Thermal and Fluid Science, 29(6), 685-96. doi:10.1016/j.expthermflusci.2004.11.001.
8. Lee KS, Kim WS, Lee TH (1997). A one-dimensional model for frost formation on a cold flat surface. International Journal of Heat and Mass Transfer, 40(18), 4359-65. doi:Doi 10.1016/S0017-9310(97)00074-4.
9. Na B, Webb RL (2004). New model for frost growth rate. International Journal of Heat and Mass Transfer, 47(5), 925-36. doi:10.1016/j.ijheatmasstransfer.2003.09.001.
10. Léoni A, Mondot M, Durier F, Revellin R, Haberschill P (2016). State-of-the-art review of frost deposition on flat surfaces. International Journal of Refrigeration, 68, 198-217. doi:10.1016/j.ijrefrig.2016.04.004.
11. Yang D-K, Lee K-S (2005). Modeling of frosting behavior on a cold plate. International Journal of Refrigeration, 28(3), 396-402. doi:10.1016/j.ijrefrig.2004.08.001.
12. Yang D-K, Lee K-S, Cha D-J (2006). Frost formation on a cold surface under turbulent flow. International Journal of Refrigeration, 29(2), 164-9. doi:10.1016/j.ijrefrig.2005.07.003.
13. Lenic K, Trp A, Frankovic B (2009). Transient two-dimensional model of frost formation on a fin-and-tube heat exchanger. International Journal of Heat and Mass Transfer, 52(1-2), 22-32. doi:10.1016/j.ijheatmasstransfer.2008.06.005.
14. Cui J, Li WZ, Liu Y, Jiang ZY (2011). A new time- and space-dependent model for predicting frost formation. Applied Thermal Engineering, 31(4), 447-57. doi:10.1016/j.applthermaleng.2010.09.022.
15. Cui J, Li WZ, Liu Y, Zhao YS (2011). A new model for predicting performance of fin-and-tube heat exchanger under frost condition. International Journal of Heat and Fluid Flow, 32(1), 249-60. doi:10.1016/j.ijheatfluidflow.2010.11.004.
16. Kim D, Kim C, Lee K-S (2015). Frosting model for predicting macroscopic and local frost behaviors

on a cold plate. International Journal of Heat and Mass Transfer, 82, 135-42. doi:10.1016/j.ijheatmasstransfer.2014.11.048.
17. Wu X, Ma Q, Chu F, Hu S (2016). Phase change mass transfer model for frost growth and densification. International Journal of Heat and Mass Transfer, 96, 11-9. doi:10.1016/j.ijheatmasstransfer.2016.01.018.
18. Xia B, Liang X, Xu X (2020). Experimental research on frosting behavior of cold plate under high speed air flow. J Eng Them, 41(8), 2031-5.
19. Carey VP. (2007). Liquid-Vapor Phase-Change Phenomena : an introduction to the thermaphysics of vaporization and condensation processes in heat transfer equipment. Boca Raton: CRC.

Figures

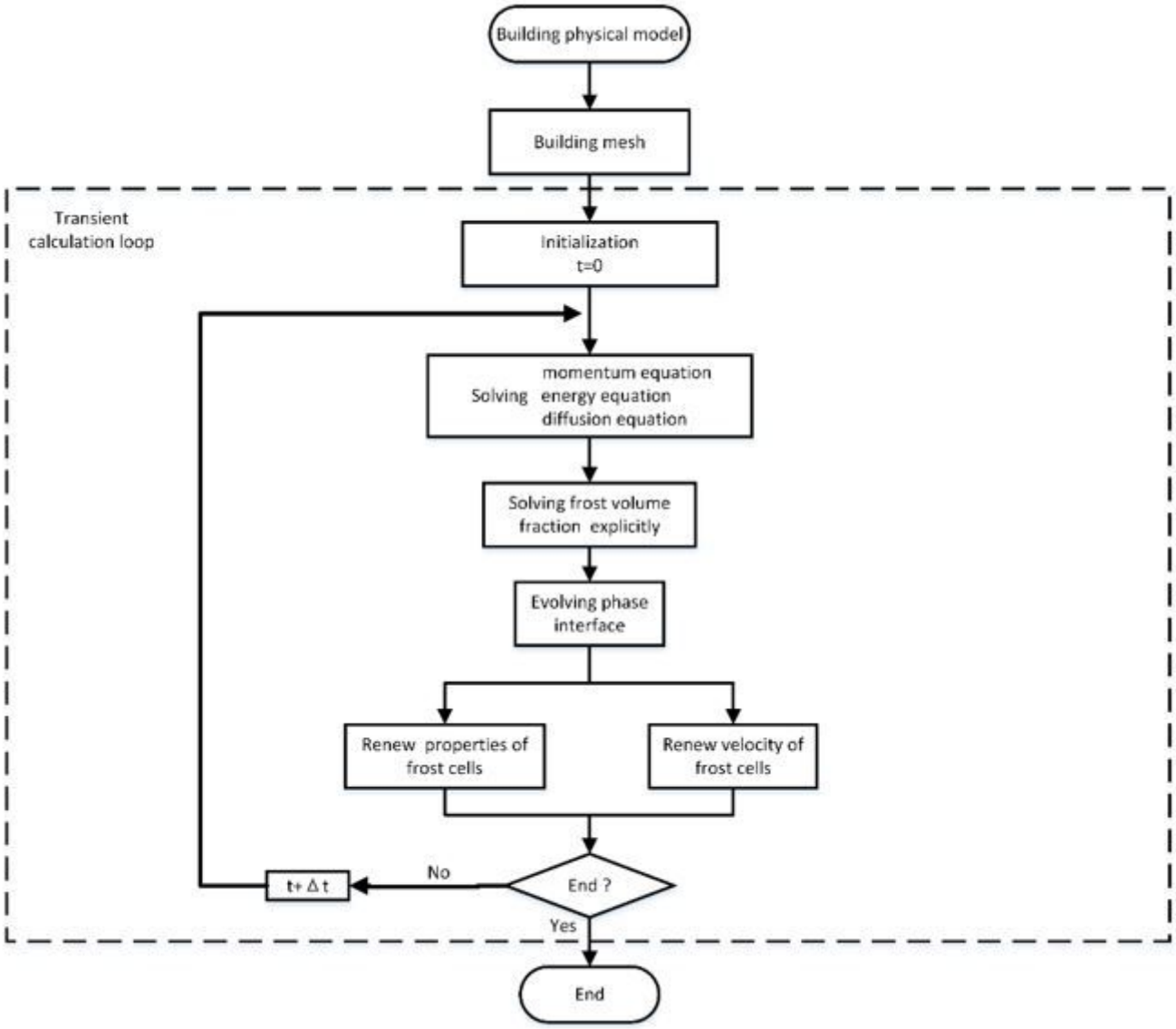

Figure 1

Flow chart of simulation

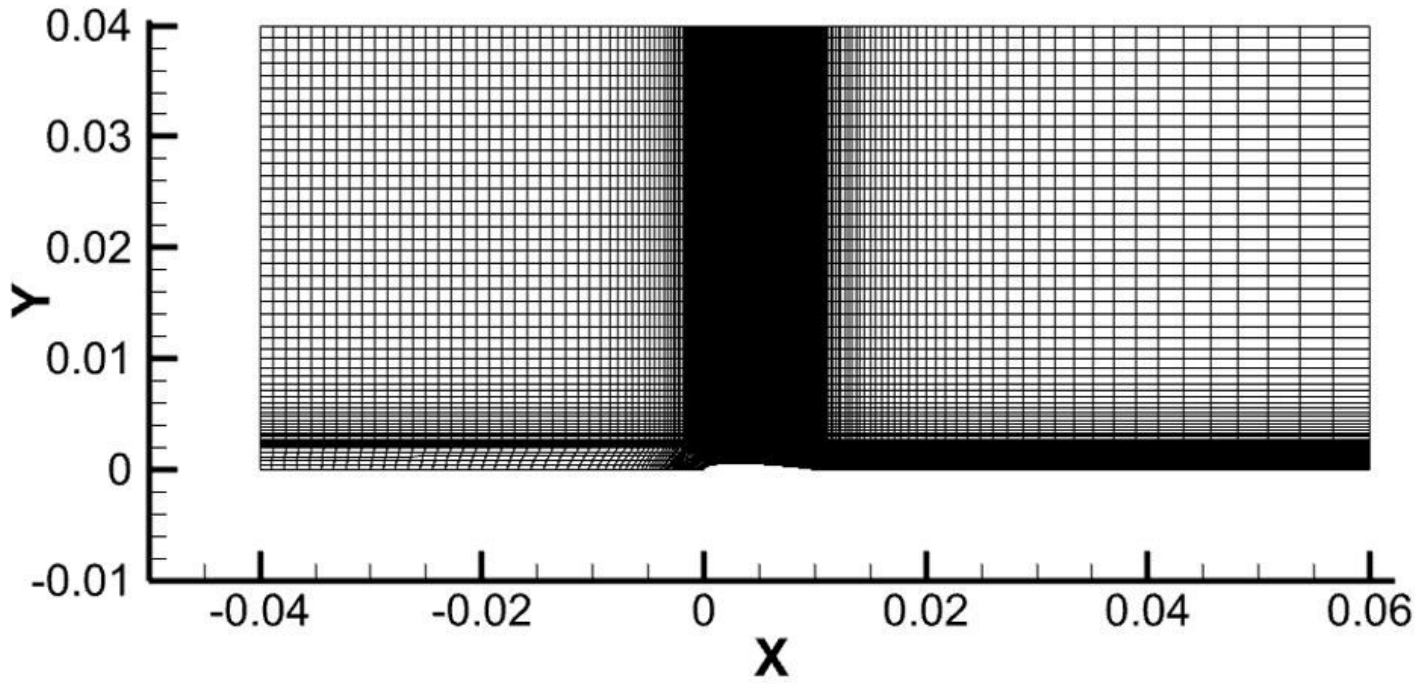

Figure 2

Mesh for frosting simulation on airfoil

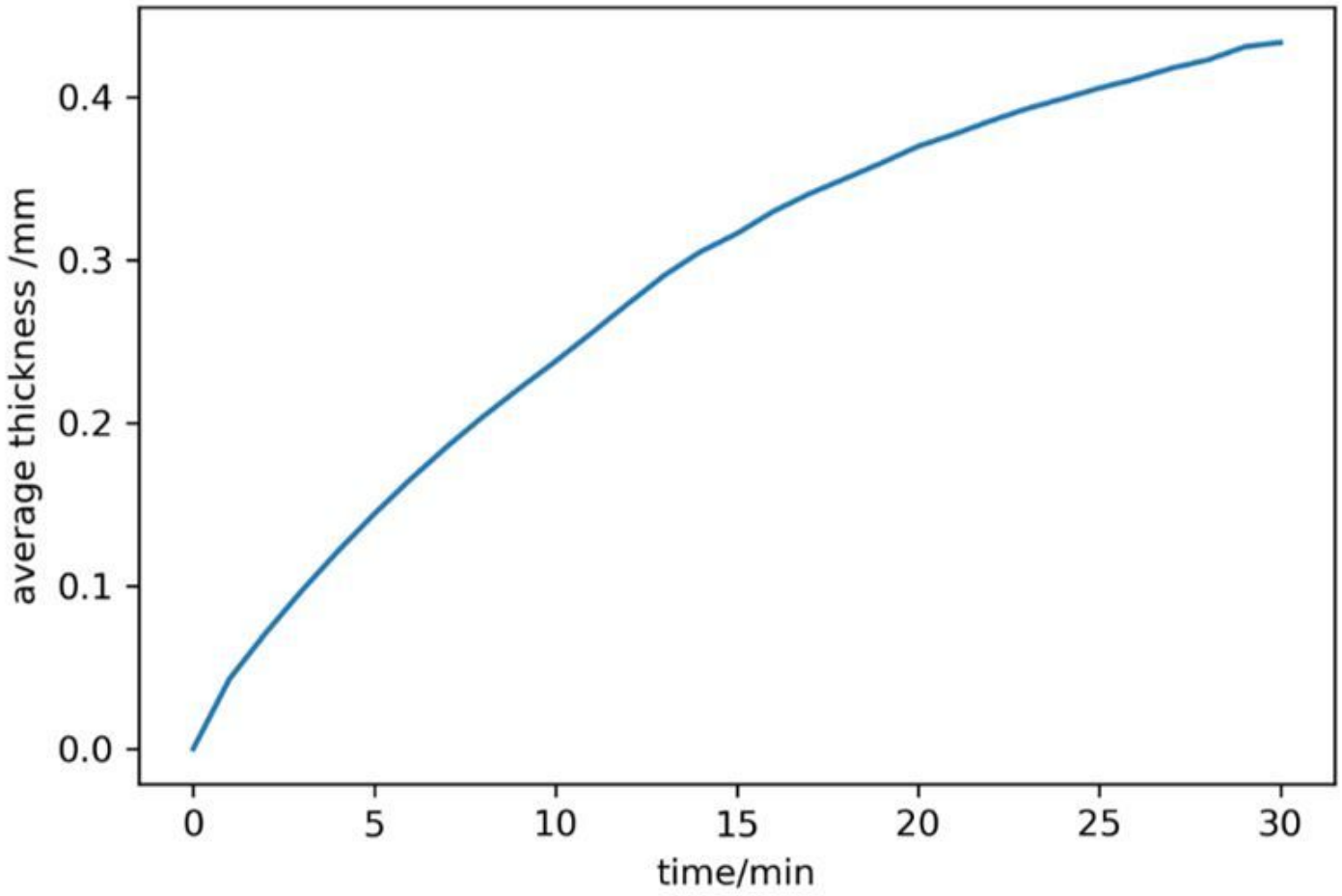

Figure 3

Average frost layer thickness varying with time under baseline state condition

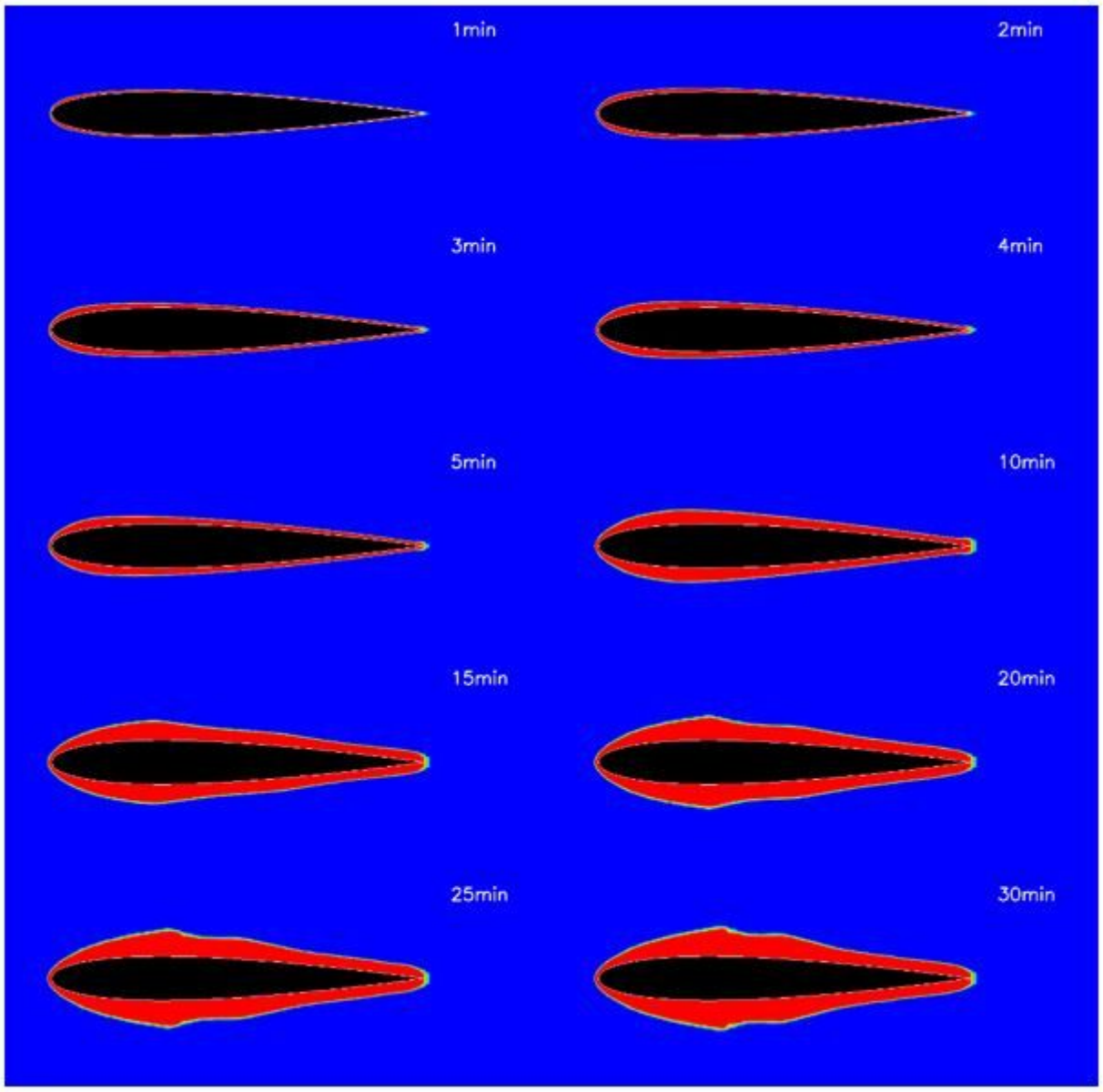

Figure 4

The morphology of the frost layer on the airfoil varying with time

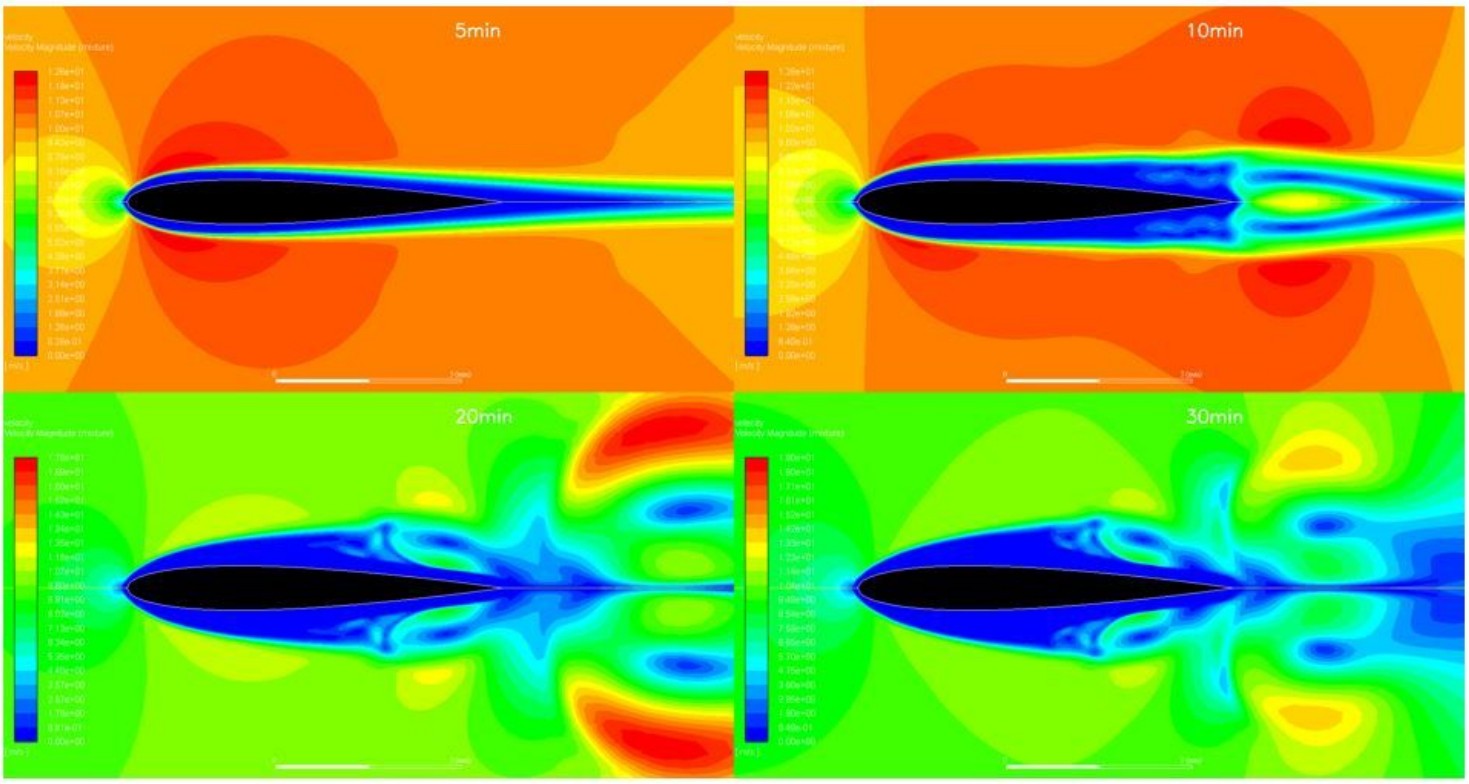

Figure 5

Velocity field changes with the frosting on airfoil

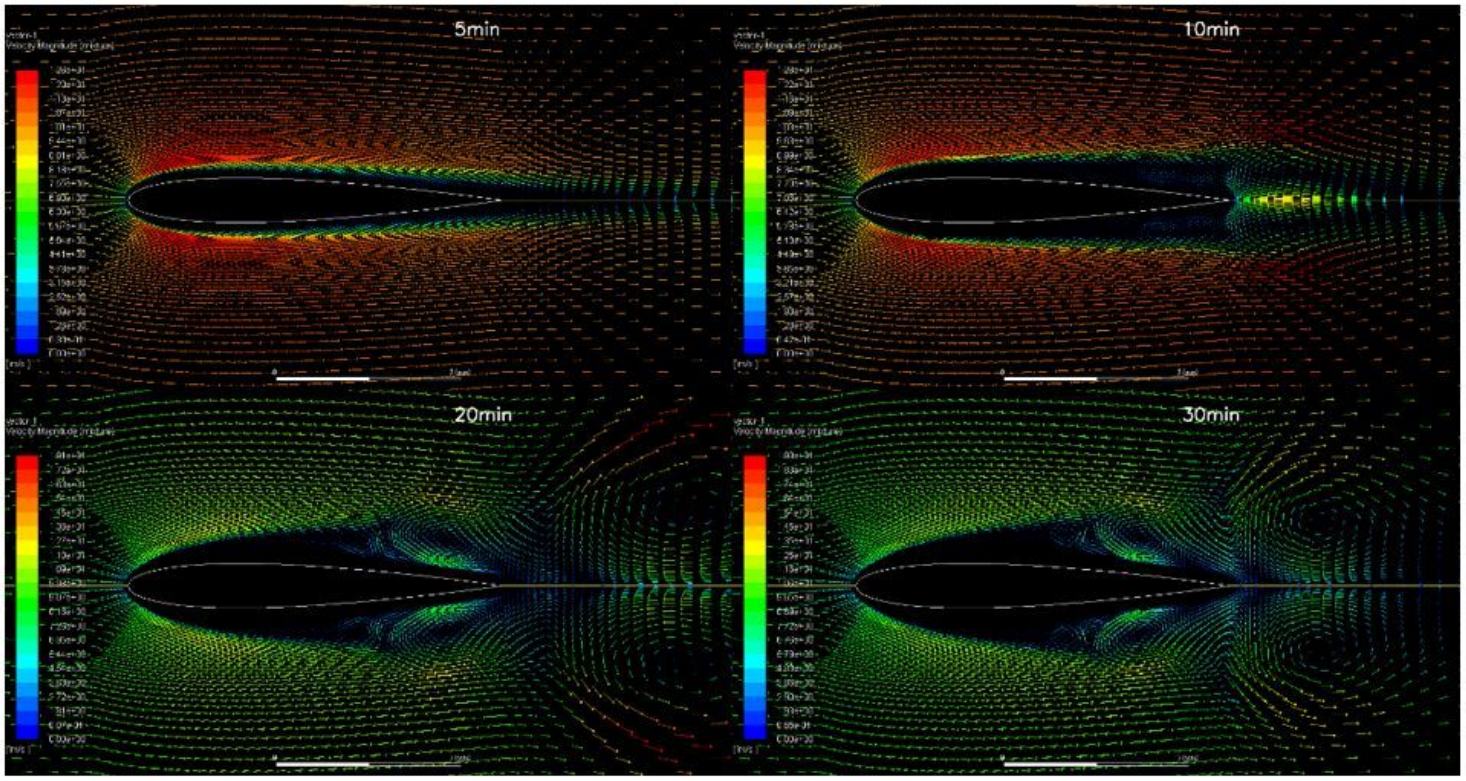

Figure 6

Velocity vector field changes with the frosting on airfoil

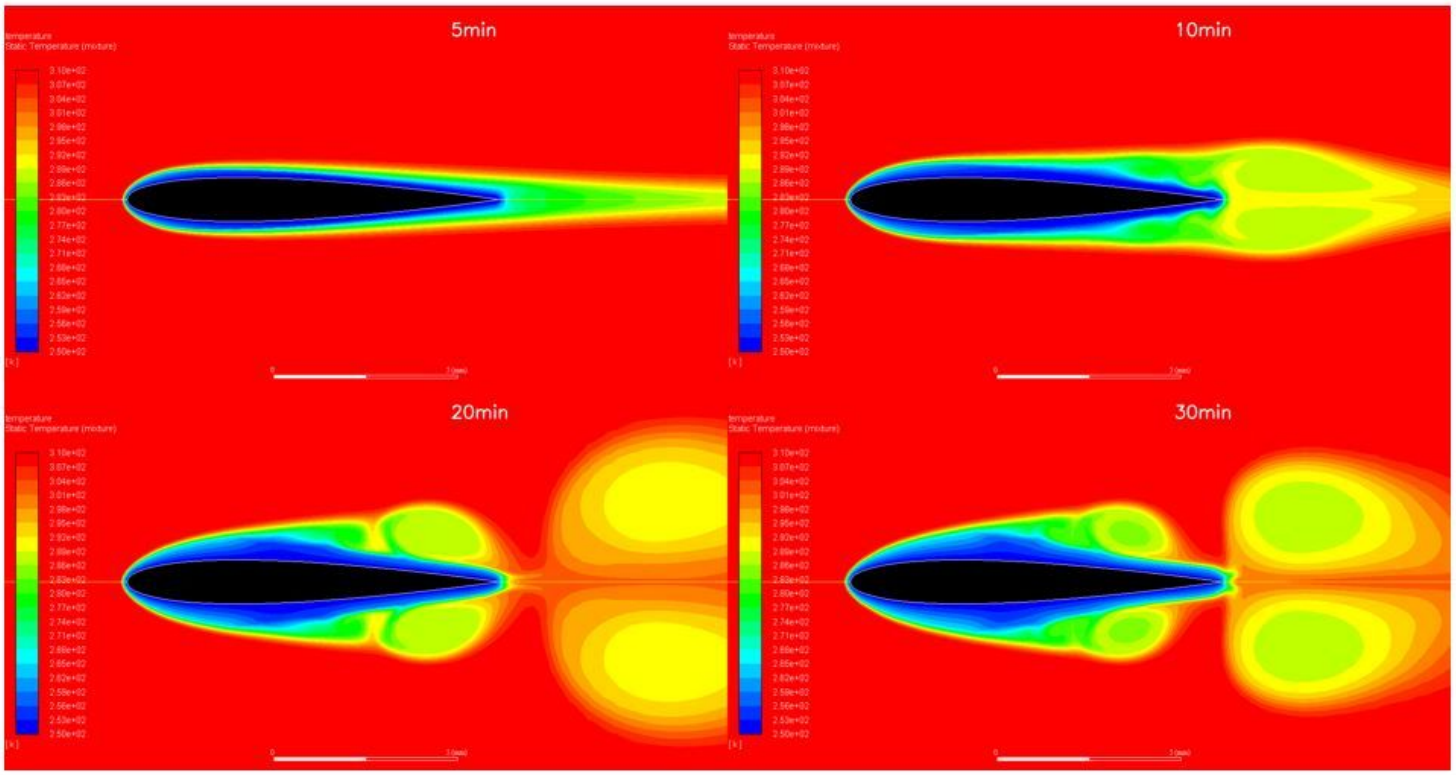

Figure 7

Temperature field of two-dimensional airfoil surface varying with time

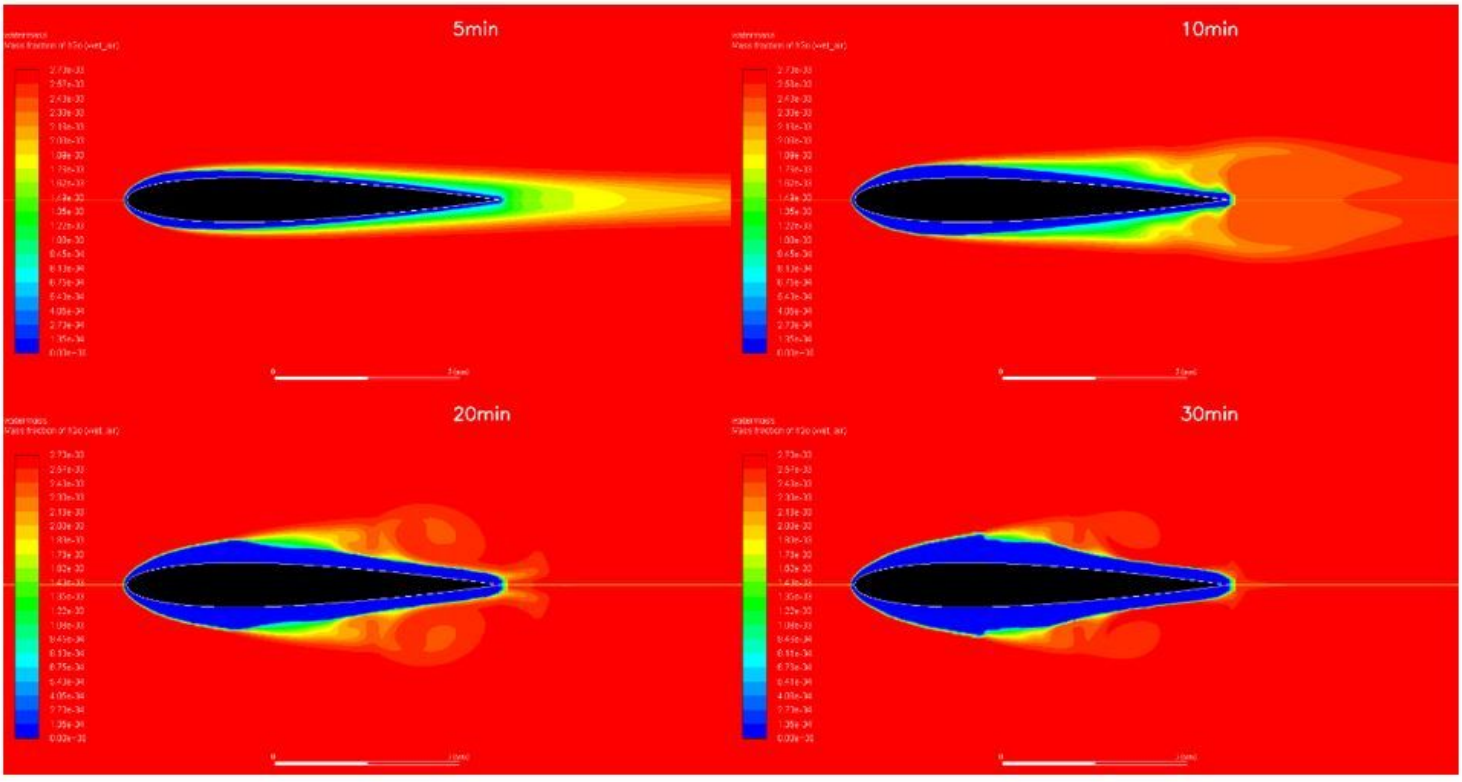

Figure 8

Water vapor content change in the air with the frosting on airfoil

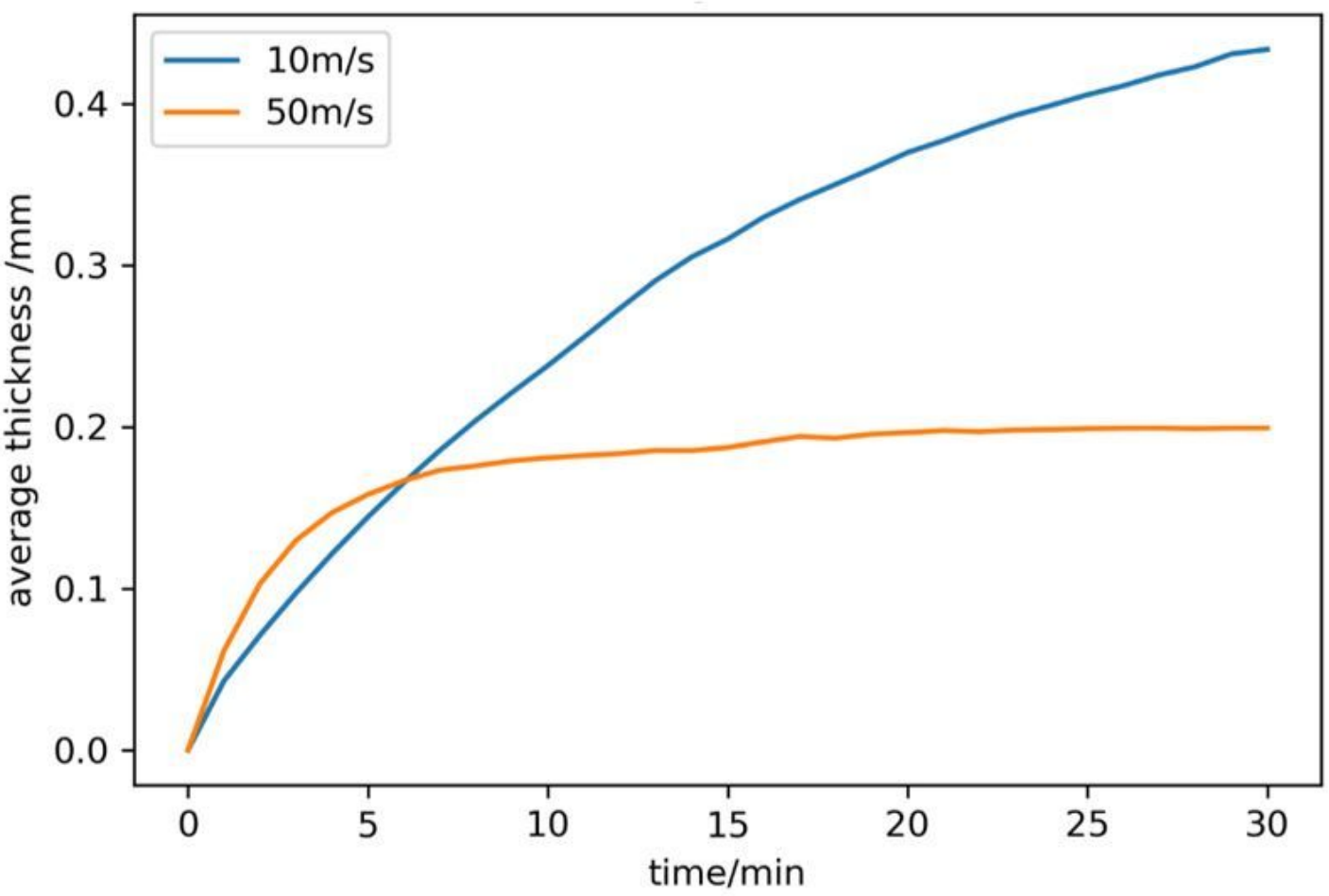

Figure 9

Variation of the average thickness of the frost layer under different air velocities

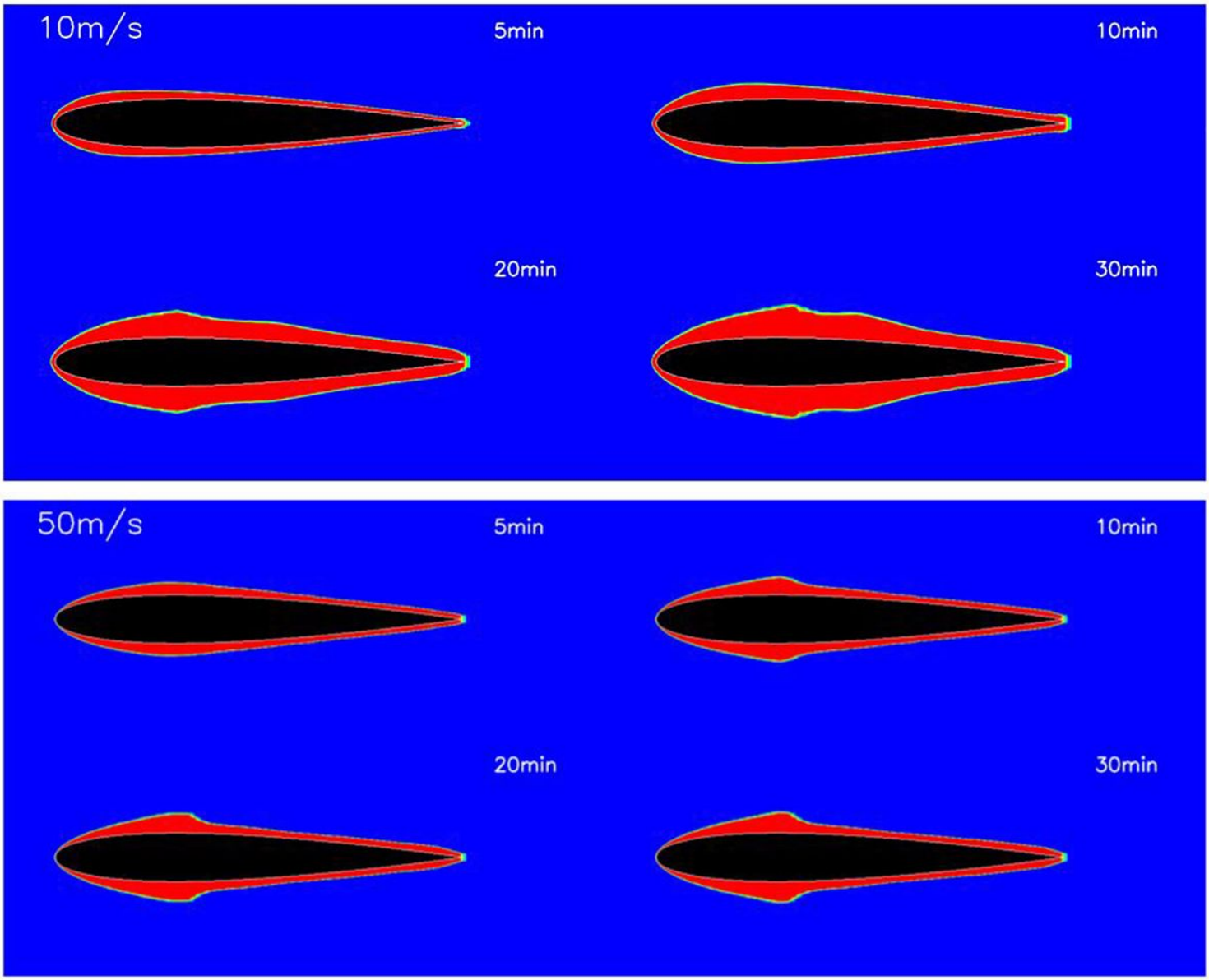

Figure 10

Frost layer morphology varying with time under different air velocities

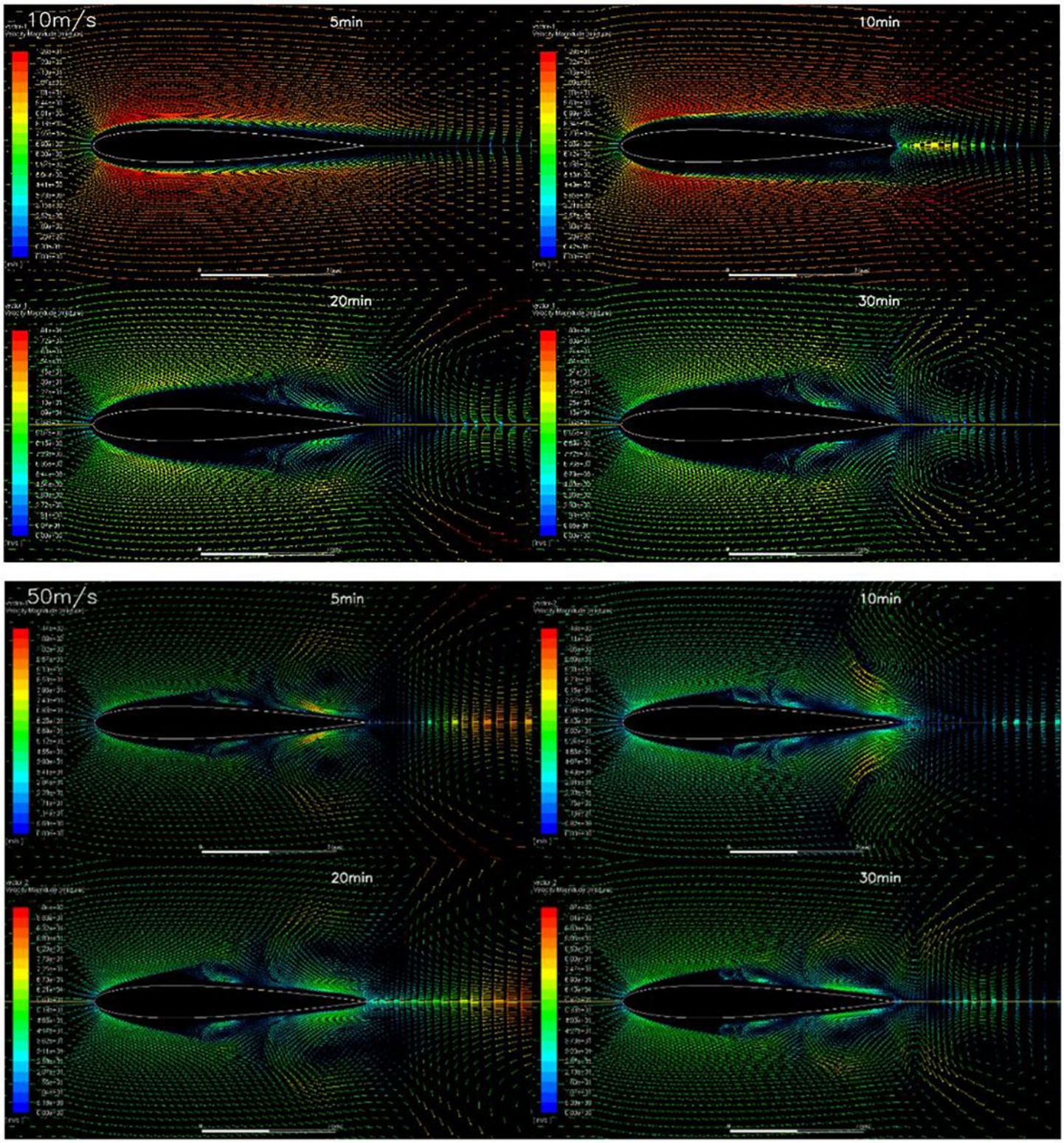

Figure 11

Velocity vector field varying with time under different air velocities

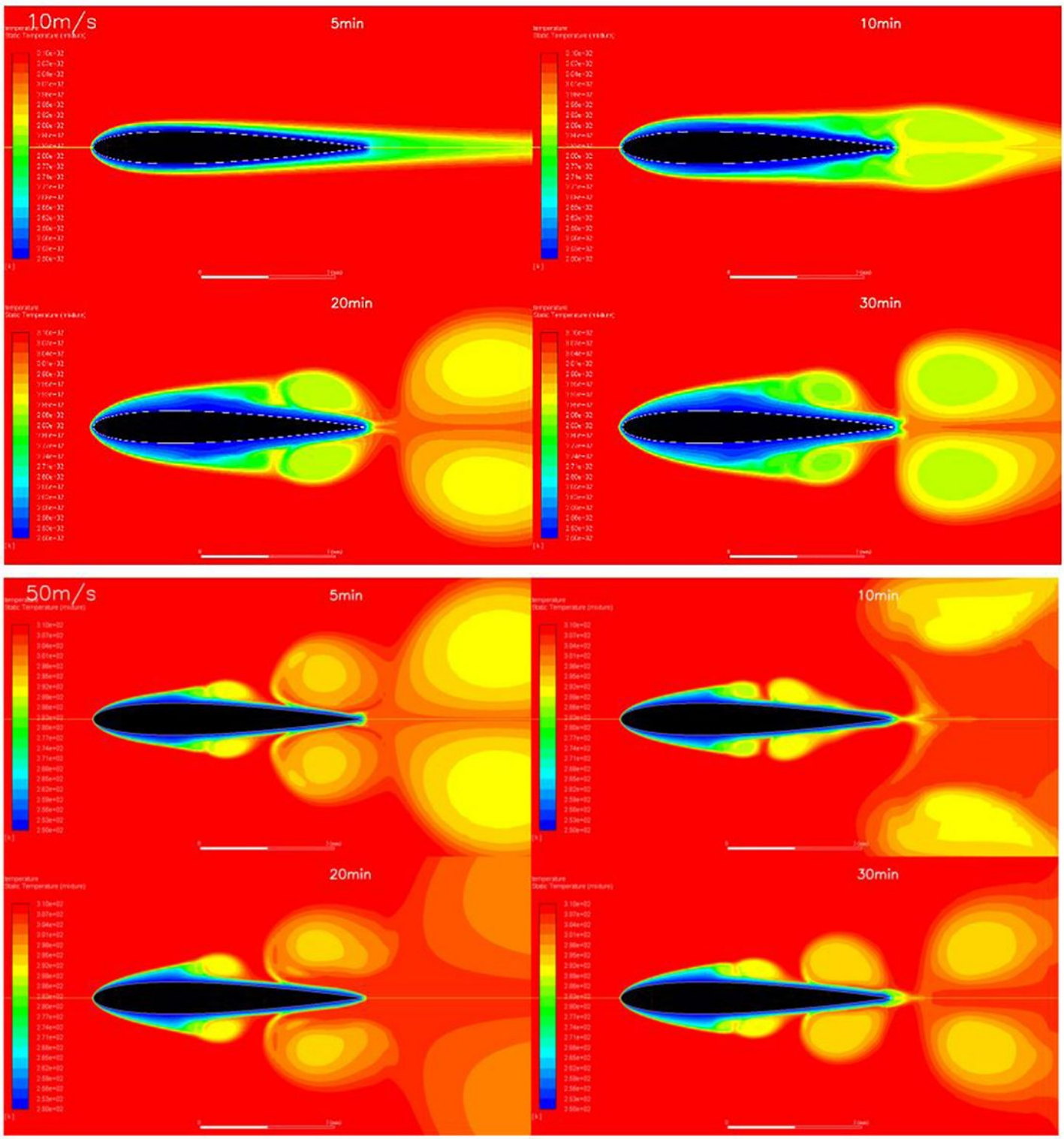

Figure 12

Temperature field varying with time under different air velocities

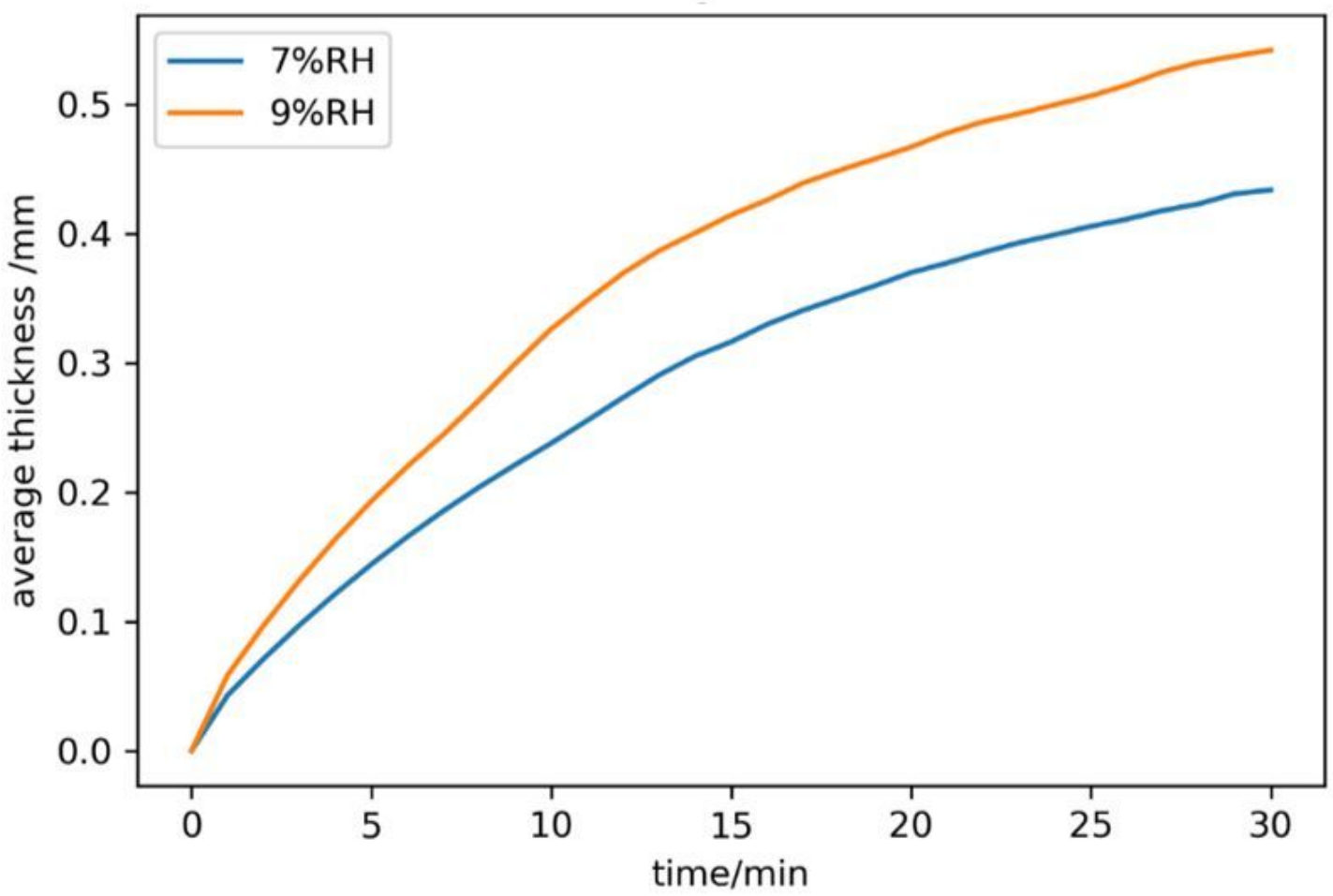

Figure 13

Change in average frost thickness with time under different air humidity

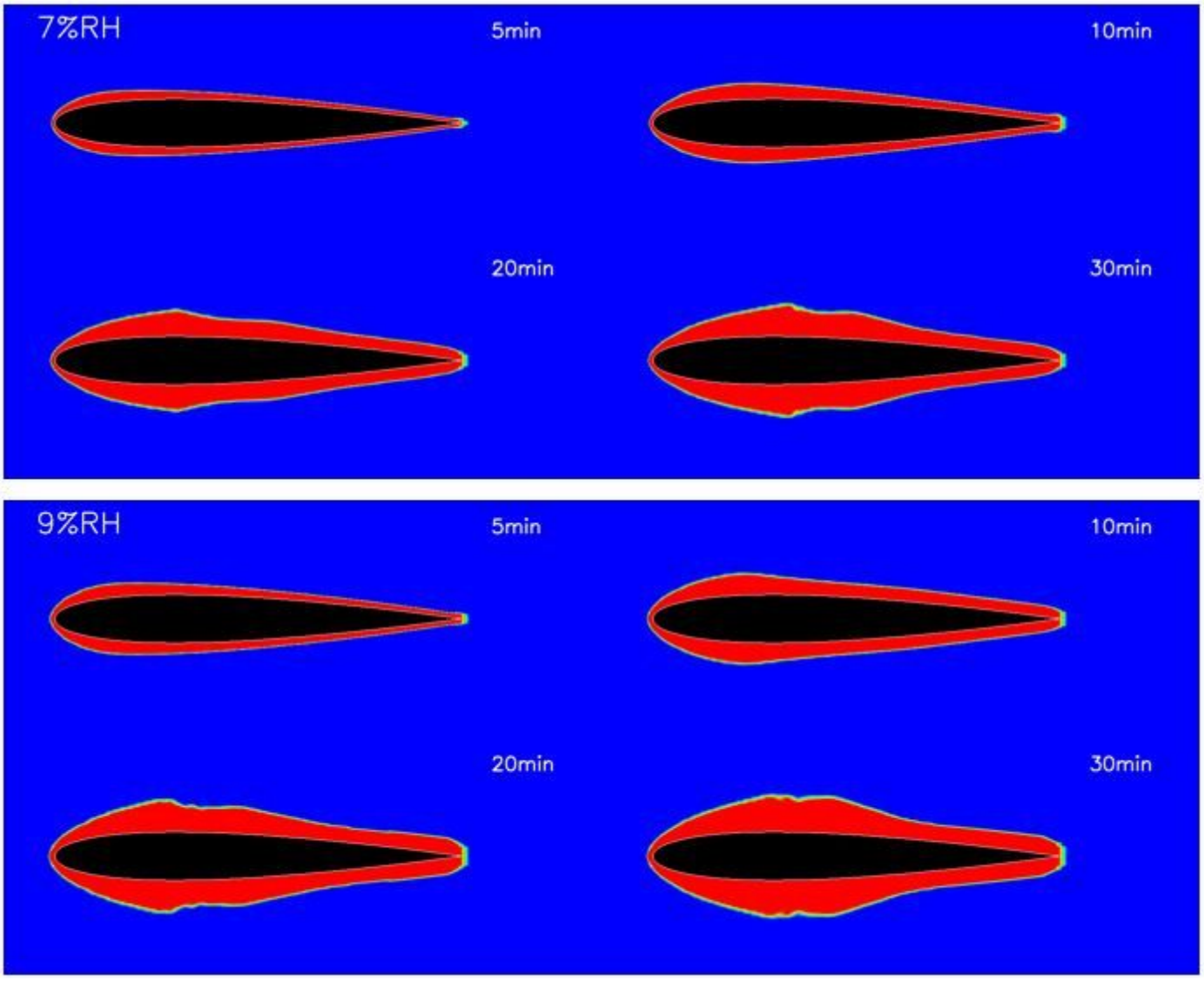

Figure 14

The morphology change of the frost layer with time under different humidity

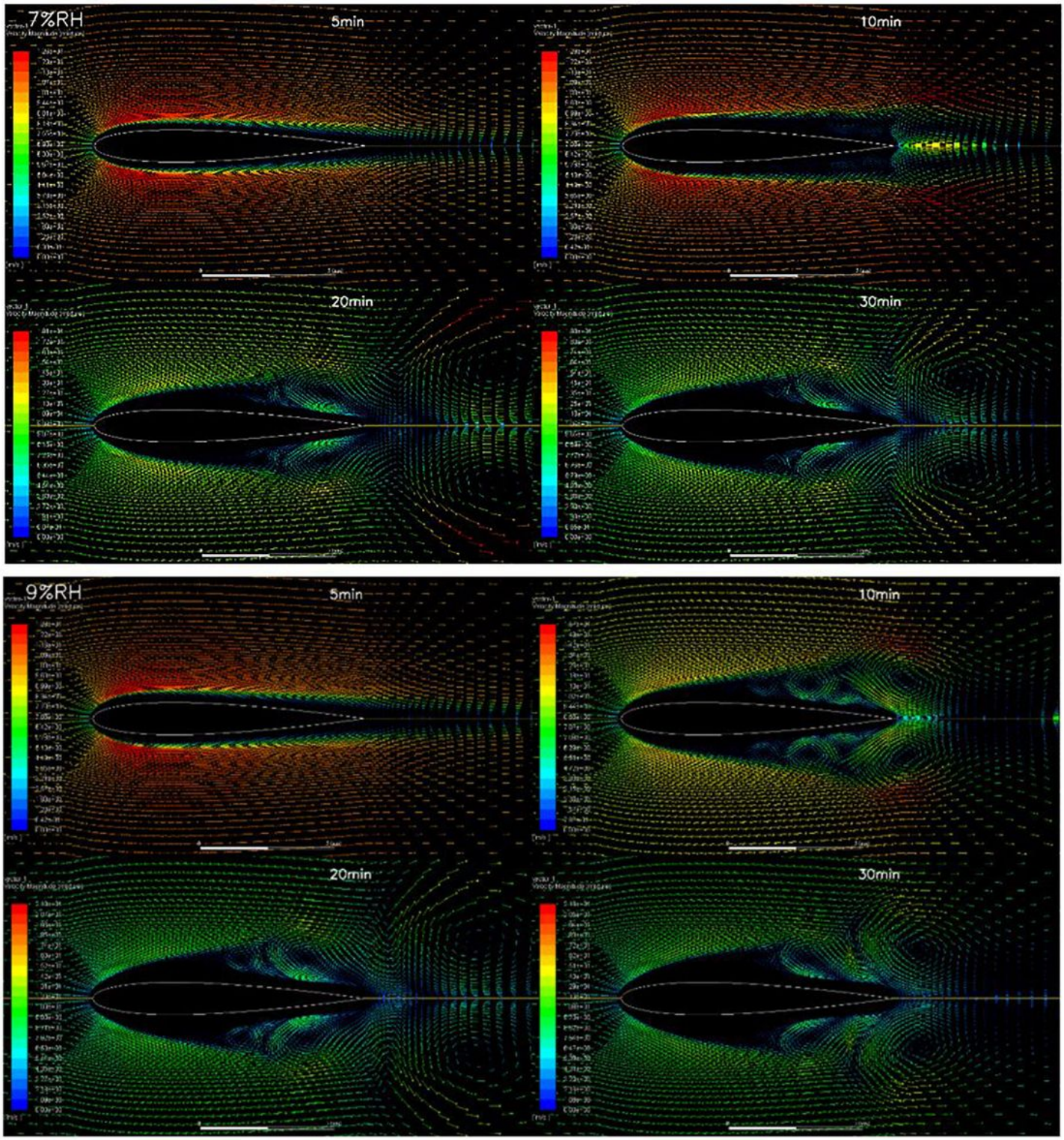

Figure 15

Velocity vector field varying with time under different air humidity

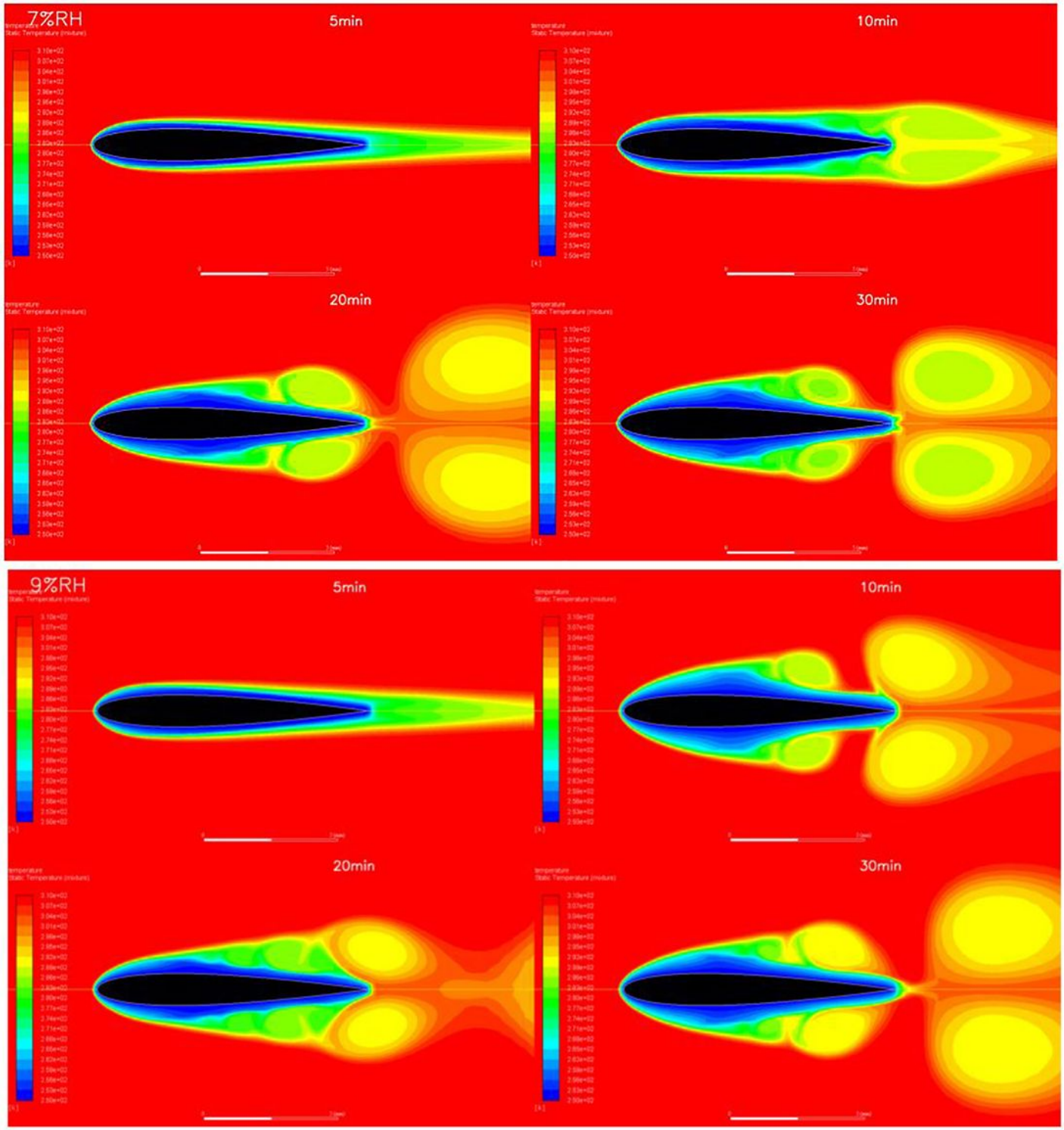

Figure 16

Change of temperature field with time under different humidity conditions

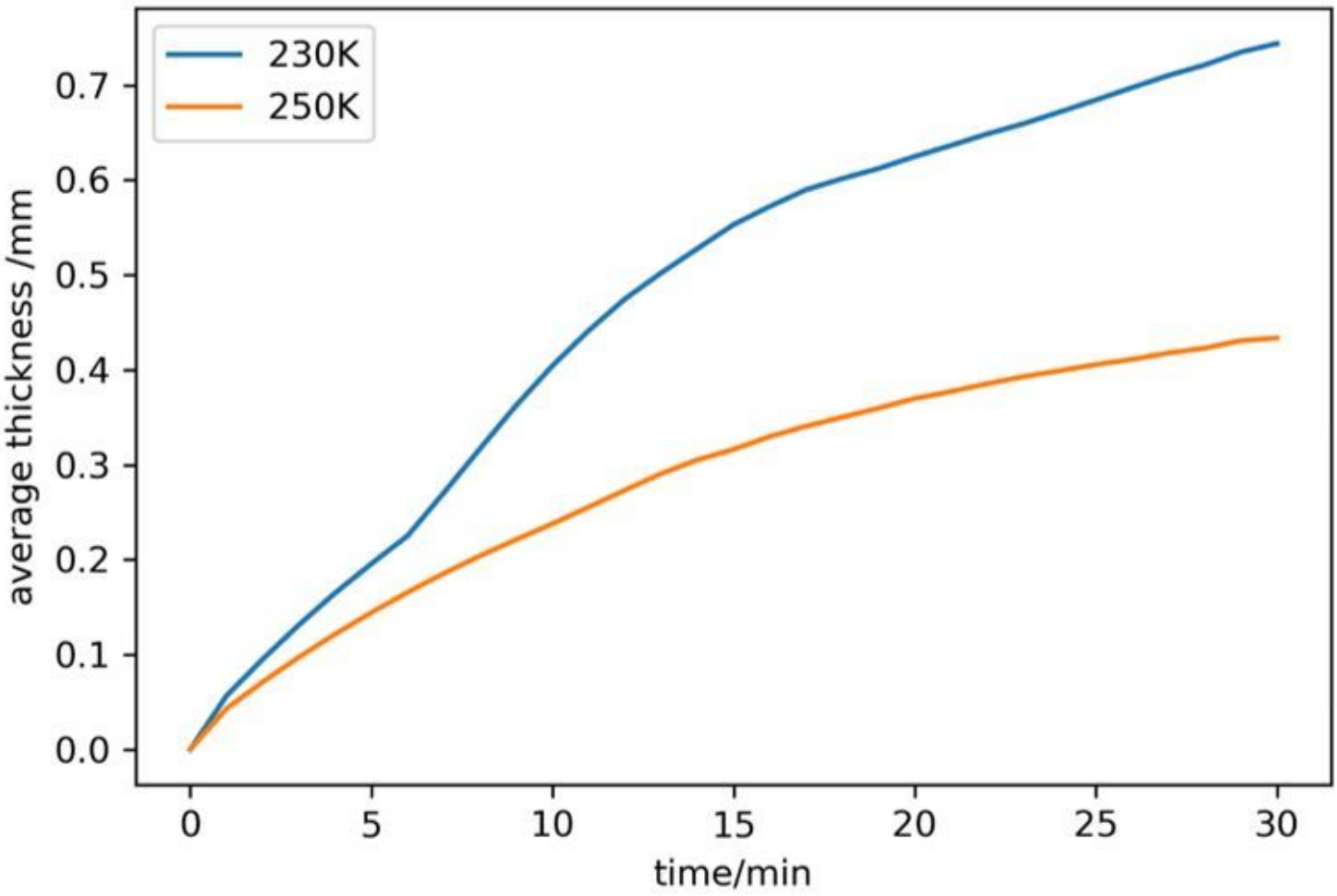

Figure 17

The change of average frost thickness time under different airfoil surface temperatures

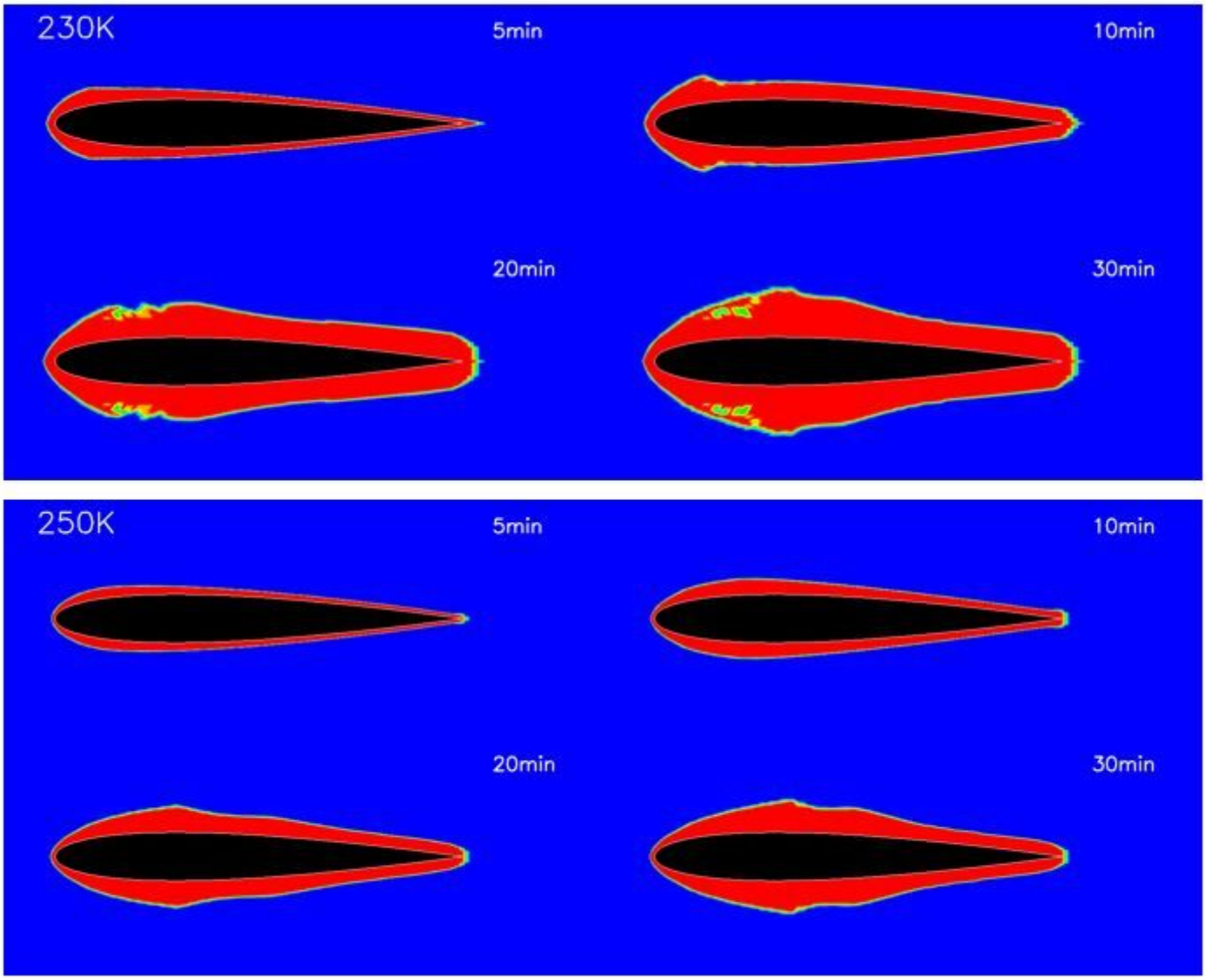

Figure 18

The morphology of the frost layer varying with time under different airfoil surface temperatures

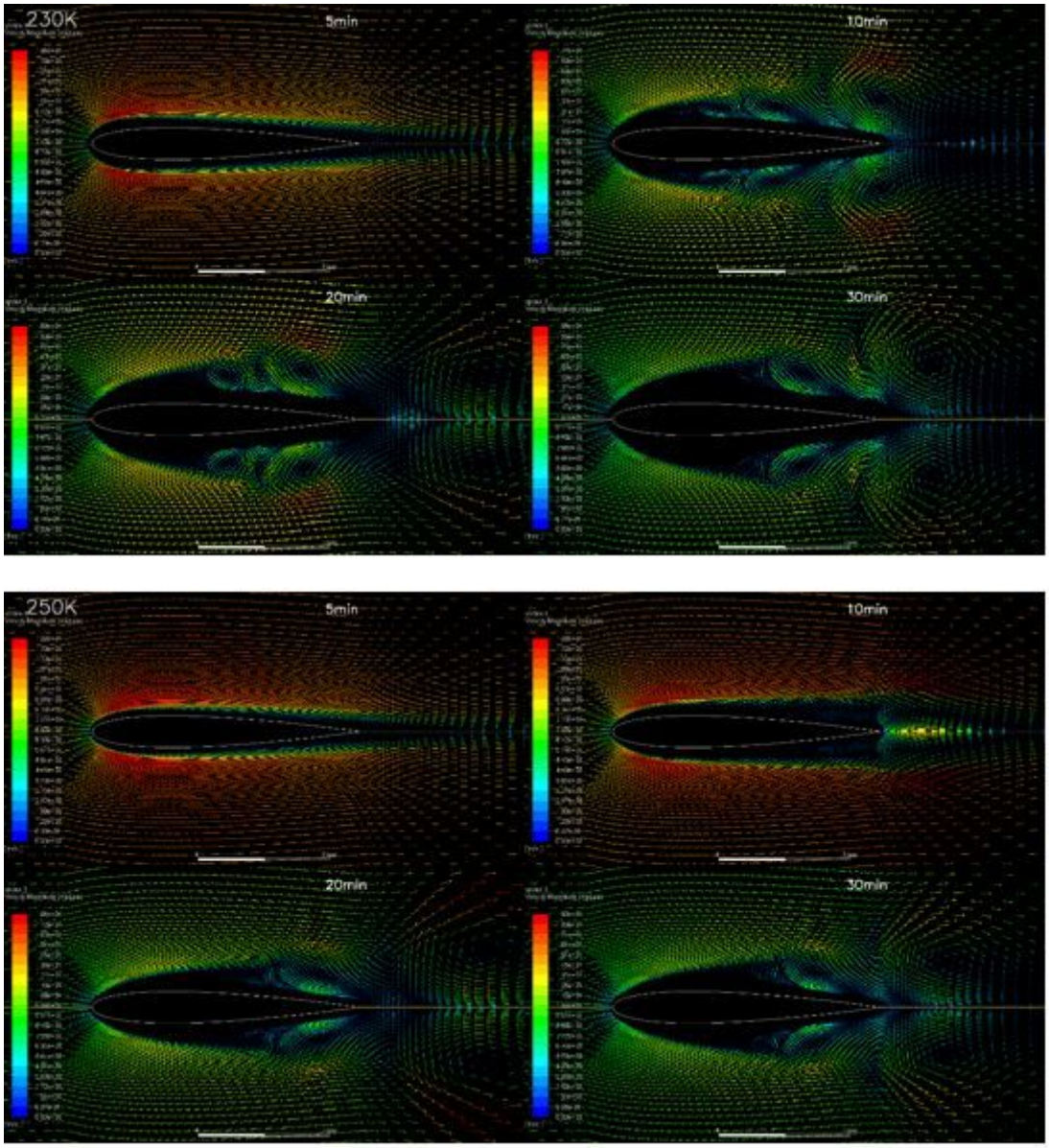

Figure 19

Velocity vector field varying with time under different airfoil surface temperatures

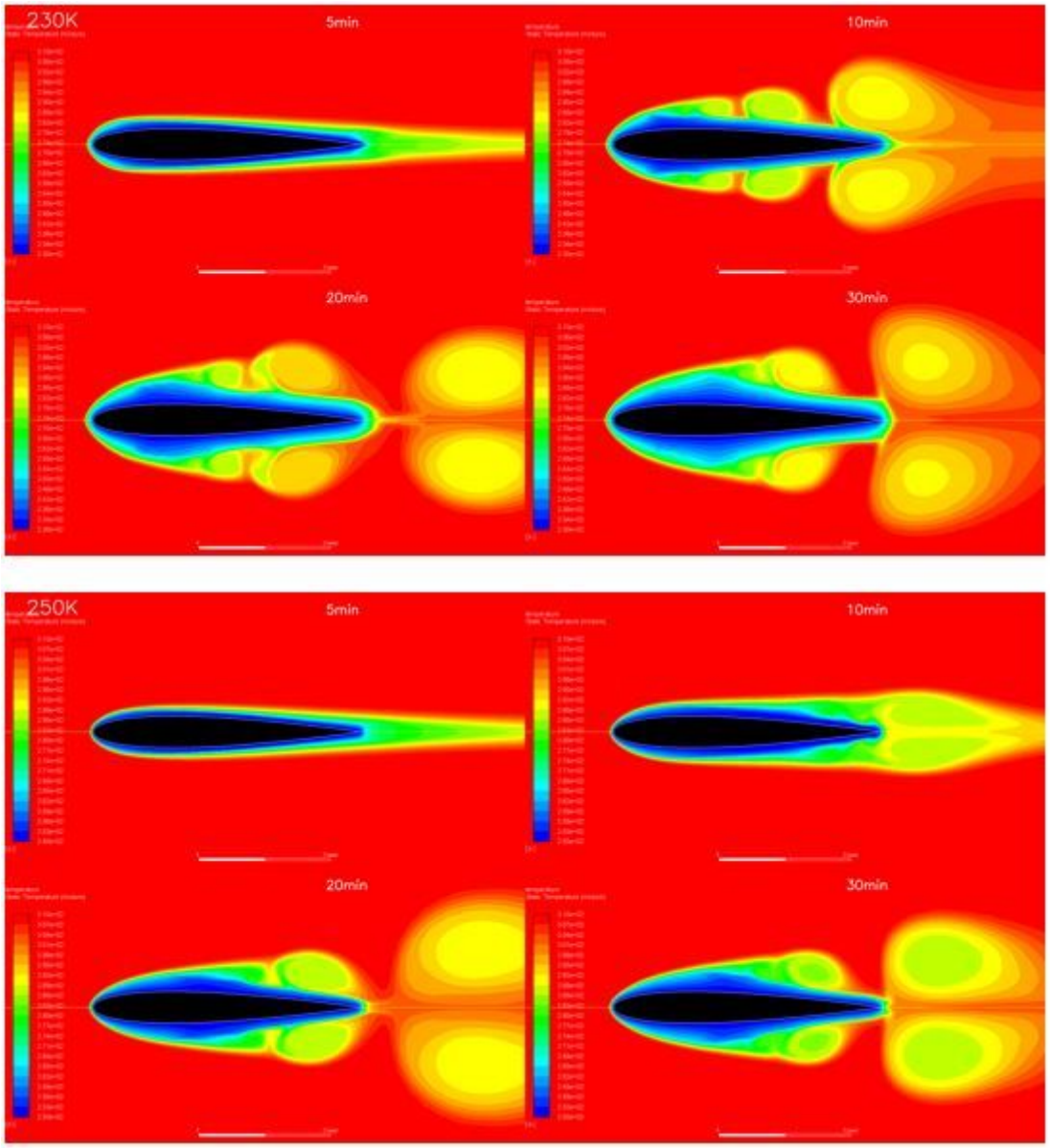

Figure 20

Temperature field varying with time under different airfoil surface temperature